

NOTE

CEA-IRFU-SIS
CERN-AT-MCS
RAL-STFC
LBNL

Date: May 29 2009
v 1.0

EDMS Id: 1001930
CEA N/Ref: IRFU/SIS/1753/09/PM

NED Short Model Coils project: Technical Note on Mechanical Design

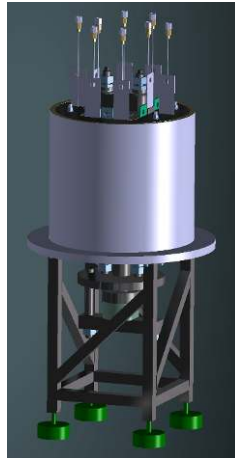
Pierre Manil¹, Federico Regis²,
Marta Bajko², Elwyn Baynham³, Simon Canfer³, Shlomo Caspi⁴, George Ellwood³, H el ene F elice⁴,
Paolo Ferracin⁴, Paolo Fessia², Peter Ford³, Ray Hafalia⁴, Juan Carlos Perez², Gijsbert de Rijk²

¹ CEA/DSM/IRFU/SIS, Gif-sur-Yvette, France

² CERN/TE, CH-1211 Gen eve 23, Switzerland

³ RAL/STFC, Harwell Science and Innovation Campus, Didcot, United Kingdom

⁴ LBNL, UC Berkeley, California, United States



Abstract

The **Short Model Coils** working group was set in February 2007 within the context of the Next European Dipole (NED) Joint Research Activity. The aim of the collaborative program is to design, manufacture and test 13 T Nb₃Sn racetrack subscale coils in dipole configuration. An adapted support structure will be used to perform training studies while investigating pre-stress influence on coil behaviour and quench triggering. It needs to have the ability to apply very high as well as very low pre-stresses on the coil pack, in the three directions. Such a system should help define the mechanical stress limit on different coil pack configurations with innovative insulations. SMC studies will utilise the experience of Berkeley's SD01 subscale coil, which is pre-stressed by a shell-based structure and is using bladders and keys.

The initial magnetic optimization phase has led to validate the SMC coil pack properties and the corresponding expected field. This paper details the support structure design, from baseline concepts to structural assessment and variable stress management. Dimensioning computations and results (in 2D and 3D) are presented first, before justifying the detailed geometrical choices for the assembly. Associated tooling such as bladders and jacks is also described in details.

This mechanical design phase has led to validate the SMC structure, so that it can be used with different coil pack dimensions and so that it enables to control precisely the target pre-stress in the three directions.

Contents

1-	Overview of the <i>Short Model Coils</i> project	Page 3
1.1	Goal of the project	3
1.2	Magnetic optimization results	4
1.3	Mechanical specifications	5
1.4	Steps	6
2-	Mechanical Principle	7
2.1	Assembly architecture	7
2.2	Pre-stress application	8
3-	Conceptual Design	9
3.1	Material properties	9
3.2	Parameters	10
3.3	Simulation codes	11
	a. CAST3M	11
	b. ANSYS	12
3.4	2D Results	13
	a. CAST3M	13
	b. ANSYS	15
3.5	Simplified 3D Results with CAST3M	17
3.6	3D Results with CAST3M	18
	a. Coil behaviour analysis	18
	b. Structure analysis	19
3.7	3D Results with ANSYS	22
	a. Model description	22
	b. Parametric analysis of the longitudinal pre-load	23
	c. Final configuration	24
4-	Detailed Design	31
4.1	Structure	31
	a. Sub-elements	31
	b. Parts shape	31
	c. Machining tolerances	33
	d. Validation	33
4.2	Bladders	34
	a. Series 1	34
	b. Series 2	35
4.3	Support and cryostat	37
4.4	Installation procedure	37
5-	Conclusions and next steps	38
	Acknowledgements	38
	Tables and figures	39
	Acronyms and symbols	40
	References	41

1- Overview of the Short Model Coils project

1.1- Goal of the project

Particle accelerators are key tools for particle physics, as they allow researchers to explore smaller and smaller components of matter by colliding elementary particles at very high energies. The beam energy is proportional to the curvature radius, which depends on the magnetic field created by dipole magnets. To reach the very high magnetic fields required to produce the high energies of collision, superconducting materials are used. Their lack of electrical resistance at low temperatures makes the use of very high current densities possible. As an example, the Large Hadron Collider (LHC) at CERN will reach collision energies of a magnitude of 14 TeV thanks to NbTi dipoles producing a field higher than 8 T in a 56 mm aperture.

Future LHC upgrades requiring higher fields in larger apertures will demand the use of a superconductor with greater performance compared to NbTi. The use of Nb₃Sn is one possibility, allowing peak fields in the conductor up to 24 T to be sustained. However, this material remains very sensitive to mechanical constraints. Its upper working stress limit, which is estimated around 150 MPa, is not precisely known. Furthermore, the behaviour of Nb₃Sn cables in wound coils is not fully understood.

The goal of the Short Model Coils (SMC) working group, within the CARE NED¹ context, is to create a short-model Nb₃Sn coil testing device [1].

The function of this device is the application of variable pre-stress levels to the coil in order to study the degradation of the magnetic properties of the superconducting cable due to different levels of stresses. The use of bladders and keys has been retained from Berkeley's SD01 coil, to provide an adequate on-plane pre-stress [2,3,4]. The longitudinal pre-stress will be applied by means of rods. Another requirement is the device needs to be easy to assemble and disassemble, to allow the testing of different types of cable in the subscale racetrack test dipoles. Additionally the SMC wishes to test different conductor insulation methods *i.e.* so-called "conventional insulation" (glass fibre + organic matrix), and more innovative ceramic insulation [5].

The SMC group will supervise the design and manufacture of the coils to be tested, of their support and testing structure and of the associated tooling. The SMC group comprises four laboratories: CERN/AT-MCS (CH), RAL (UK), CEA/IRFU/SIS with support from CEA/IRFU/SACM (FR) and LBNL (US). The mechanical optimization of the structure has been mainly supervised by CERN and CEA whereas RAL has focused on the coil pack fabrication process. This paper concentrates on the structural design.

¹ NED is an acronym for Next European Dipole. This Joint Research Activity (JRA) was launched on January 2004 to promote the development of high performance Nb₃Sn conductors in collaboration with European industry and to assess the suitability of Nb₃Sn technology to the next generation of accelerator magnets. The target is to reach a non-copper critical current density of 1500 A.mm⁻² at 4.2 K and 15 T, an aperture of 88 mm and a conductor peak around 15 T.

1.2- Magnetic optimization results

The magnetic optimization steps are presented in the **Technical Note on Magnetic Design [6]**. This preliminary study has led to a successful design with the below-mentioned characteristics. The dipole magnet consists in the assembly of two identical double pancakes, as showed:

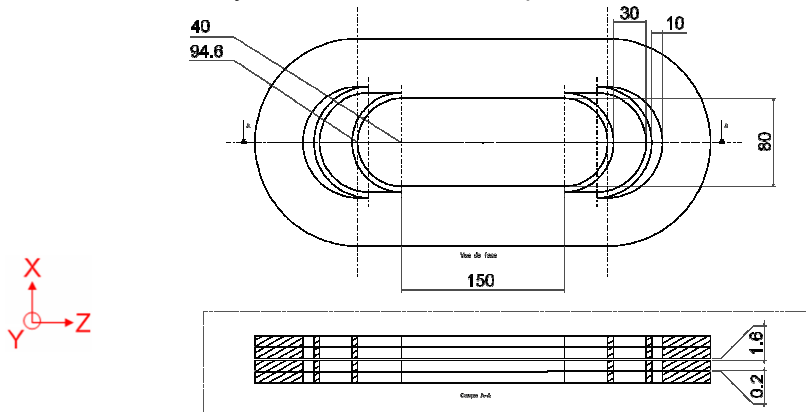


Fig. 1.2.1: SMC magnet optimized geometry [in mm]

This configuration is associated with surrounding iron parts that help concentrate the field around the straight section. Our magnetic models have been implemented on the base of provisory iron parts profiles. Thus, let's point that if the coil pack properties are definitely fixed, some minor changes may happen on the iron parts shape during the mechanical optimization (§ 4.1.b). The final parameters list is the following:

Parameter	Name	Unit	Value	d.o.f. ²	Notes
Coil Pack – Double Pancake Configuration					
Turns number	N_{tot}	/	21	fixed	
Inner turns number	N_{int}	/	2	fixed	
Mid-pack turns number	N_{mid}	/	2	fixed	
Outer turns number	N_{out}	/	17	calculated	
Island half-width	r_{int}	mm	40	fixed	
Outer Radius	r_{out}	mm	94.6	calculated	
Straight section length	L	mm	150	fixed	
Interlayer thickness	e_{int}	mm	0.2	fixed	
Midplane insulation thickness	e_{mid}	mm	1.6	fixed	
2 End Spacers					
Inner spacer axial length	L_s	mm	30	fixed	
Outer spacer axial length	L_{int}	mm	10	fixed	
Coil Dimensions					
Overall length	L_{tot}	mm	419.2	calculated	
Overall width	w_{tot}	mm	189.2	calculated	
Overall thickness	e_{tot}	mm	42.4	calculated	
3D Extension of Iron					
Horizontal pad	Z_{x-pad}	mm	210	fixed	= 140% L
Vertical pad	Z_{y-pad}	mm	105	fixed	= 70% L
Yoke	Z_{yoke}	mm	105	fixed	= 70% L

Tab. 1.2.2: SMC magnetic optimization results

² The “fixed” parameters are the result of the previous magnetic optimisation. The “calculated” parameters can be deduced from the fixed ones by geometrical relations. Those relations are listed in [6].

This configuration leads to the following expected magnetic field, at short sample current ($I_{ss}=14$ kA):

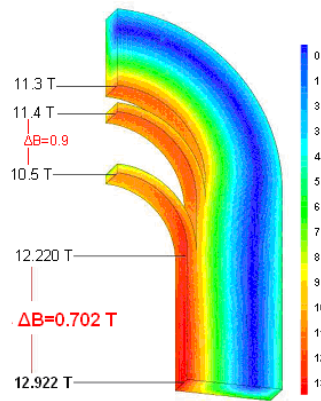


Fig. 1.2.3: SMC expected magnetic field at short sample ($I_{ss} = 14$ kA)

This plot has been realized with CAST3M, but all the magnetic results have been duly cross-checked between four formulations³. The difference observed on the field always remains below 0.3 %.

On the mechanical point of view, this field repartition leads at short sample current to consequent forces in the three directions⁴:

Lorentz forces - Energy			
X-Force on 1/8 th coil	F_x	kN	331
Y-Force on 1/8 th coil	F_y	kN	-396
Z-Force on 1/8 th coil	F_z	kN	133
X-Force on straight section	F_x^{2D}	MN.m ⁻¹	2.0
Y-Force on straight section	F_y^{2D}	MN.m ⁻¹	-1.9
Total stored magnetic energy	E_{mag}	kJ	202
Magnet inductance	\mathcal{L}	mH	2.1

Tab. 1.2.4: magnetic forces and energy at short sample ($I_{ss} = 14$ kA)

Such large forces can be damaging for the magnet. A strong support structure is necessary to control the internal stresses. Moreover, it is known that mechanical stresses strongly affect the superconducting performances of the superconducting magnets as they trigger quenches. This influence has not been fully studied on Nb₃Sn dipoles. **Thus, our structure will play a double role: managing the magnet internal stresses so that it can reach the target fields, and being a test station to investigate the pre-stress influence on quench triggering.**

1.3- Mechanical specifications

The main design criteria of the SMC support structure are:

1. Mechanical sustainability; variability of the pre-stress
2. Easiness of mounting and testing
3. Using the support with different coil packs
4. Adapted instrumentation

This paper concentrates on points 1 to 3.

³ CAST3M (MSP), ANSYS (MSP and MVP) and OPERA VF (MSP) plus ROXIE without iron

⁴ Table 1.2.4 results are the mean values obtained from the four formulations

1.4- Steps

SMC study was started in February 2007. The magnetic optimization phase has taken five months before the validation of the coil pack properties. The structural design has consisted in four phases:

- 2D modelling, to validate the in-plane behaviour of the coil assembly and its baseline properties;
- 3D modelling, to integrate the longitudinal loading system;
- detailed design and drafting;
- tooling tests in parallel to validate particular elements of the design, such as bladders.

This conception program has been completed in ten months by CEA and CERN. In parallel, numerous coil realization tests have been performed, trying to explore winding and reaction issues. This part of the project has been mainly looked at by RAL. A reflexion on the coil pack instrumentation has also been driven at CERN, to make it coherent with the surrounding assembly.

2- Mechanical Principle

2.1- Assembly architecture

A similar assembly to the SMC coil test assembly has already been realized at Berkeley (LBNL) in the US. This work has been followed at CEA Saclay by H el ene F elice (PhD work, 2003-2006), who is a collaborator within the SMC working group and a LARP correspondent [7,8].

The SD01 goal was to study the pre-stress influence on Nb₃Sn dipole magnets, and how this affected their training. Pre-stress was applied in the lateral and longitudinal directions.

SD01 comprises five main elements: the **superconducting coil pack** (in the centre), **four pre-stress pads** (horizontal and vertical), the **surrounding yoke** (split in two halves) and **an external aluminium shell**. The cryogenic system is not illustrated since it is classical. **The SMC will borrow the same structure scheme.**

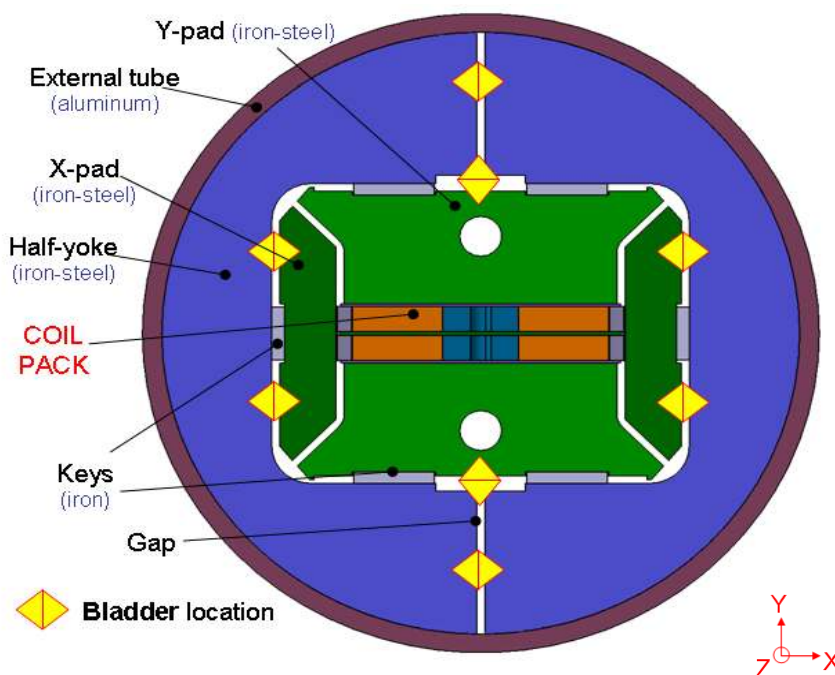


Fig. 2.1.1: SMC mechanical baseline structure (2D cut)

The pre-stress on coil is achieved through a double-step operation: part of it is provided at warm by using the bladders and keys technology developed at LBNL [2], and the remainder part is provided at cryogenic temperature by exploiting the differential in thermal contraction between components.

2.2- Pre-stress application

At warm, bladders are placed between the coil pack and the iron yoke and then inflated with pressurized water at a target pressure P_{blad} . They provide the required on-plane pre-stress (in both X and Y directions) by compressing the coil and tensioning the aluminium shell. Interference keys (including shims) then replace the bladders after they are deflated. The longitudinal pre-load (in Z direction) is provided by a couple of aluminium rods, tightened at one magnet end by a hydraulic piston.

The complementary part of the total pre-stress is then reached at cryogenic temperature by the differential in thermal contraction between the aluminium shell and rods with respect to the enclosed structure. For a fixed aluminium alloy and a fixed ΔT (289 K), the tube tension only depends on its thickness. To transfer the load at cold on the coil pack edge, we will use two half yokes separated by a 5 mm-gap designed never to come in contact. This gap is visible on figure 2.1.1.

Aim of the mechanical optimization is to find the best compromise between fixed thermal pre-stress and variable bladders pre-stress by adjusting the shell thickness and the lateral shim thickness. Finally, this architecture should enable us to reach very high and well-controlled pre-stresses in the three directions. Most of the times, we will focus on the axial and longitudinal stresses (X and Z axis). The Y-bladders will generally play a mere positioning role because of the direction of the Lorentz forces.

Extra bladders are located between the yoke halves for mounting (figure 2.1.1). They have no theoretical role and won't appear in the finite element models.

3- Conceptual Design

3.1- Material properties

The following material properties have been considered. They are based on NED values [9]. All parts have been considered as isotropic, even the insulated conductor stack. This is a rough simplification, but it appears that in our case the high stress values on coil always occur in the stack direction. Considering only the stack properties is sufficient to perform our optimizations. G10 is also modelled with its homogenized properties through thickness, since we are not interested by its behaviour in other directions.

Material	Parts	E_Y at 4.2 K	E_Y at 293 K	ν	$\int \alpha_{th} dt$ 293 – 4.2 K	ρ
		GPa	GPa	/	$m.m^{-1}$	$kg.m^{-3}$
Nb ₃ Sn (stack direction)	Insulated coil	42	30	0.30	3.9×10^{-3}	7391
NED Iron (MAGNETIL)	Y-Pads / Yoke midparts	215	205	0.30	2.1×10^{-3}	7800
Steel (316 LN)	X-Pads / Y-Pads / Yoke / Keys	204	194	0.30	2.6×10^{-3}	7800
Titanium (Ti6Al4V)	Pole / Spacers	103	103	0.36	2.8×10^{-3}	4510
Aluminium (Al 2014)	Outer tube	81.6	70	0.30	4.2×10^{-3}	2700
G10 (through thickness)	Midplane insulation / Fillers	6.4	6.4	0.30	8.0×10^{-3}	1350

Tab. 3.1.1: SMC material properties

The mechanical design aims at checking that anytime in the magnet lifecycle (pre-stress, cool-down, magnetization) the following three constraints are respected:

- every mechanical part undergo stress below the material limits (with a safety margin as showed later)
- the conductor maximum stress always remains below 150 MPa or 200 MPa in some very localized zones
- the conductor never separates from the surrounding parts (to avoid gap opening and therefore energy release).

An important result of the magnetic optimization is that we have been able to locate the peak field in the centre of the straight section, where the peak mechanical stress in conductor occurs. Therefore, we have to manage carefully the stress repartition in this zone.

3.2- Parameters

Many geometrical parameters will be discussed and adapted in next parts. Nevertheless, the overall behaviour of the structure can be precisely described by a few parameters:

- t_{shell} : the aluminium tube thickness controls after cool-down the radial stress
- r_{yoke} : the yoke radius controls the assembly stiffness
- i_x , i_y : those interference values define the shim thickness and indicate the equivalent minimum bladder pressure to provide
- i_z : this interference value simulates the longitudinal rods tightening, provided by the piston at warm

The horizontal keys, located in between the yoke and the Y-pad, only play a positioning role, so we will always have $i_y=0$ in the models. The keys width is imposed identical to the conductor width as shown on figure 3.2.1 (left).

Thus, this conceptual study will concentrate on three parameters in 2D (t_{shell} , r_{yoke} , i_x) and four in 3D (the same plus i_z).

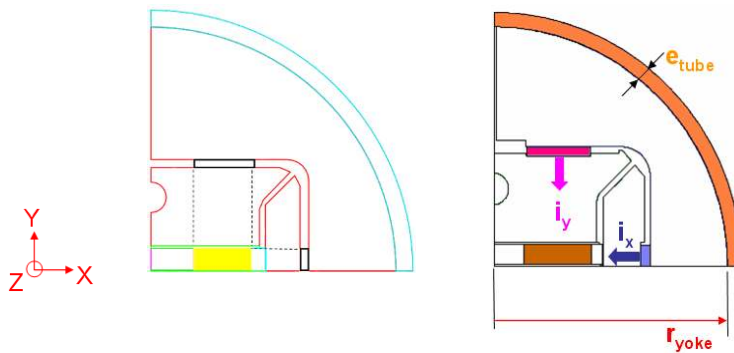


Fig. 3.2.1: SMC main parameters in 2D

3.3- Simulation codes

The mechanical optimization has been developed by Federico Regis, working with ANSYS™ at CERN, and by Pierre Manil, working with CAST3M at Saclay. In both cases, the Lorentz forces have been calculated from the nodal field components extracted from the magnetic optimization program.

a. CAST3M [10]

The CAST3M mechanical mesh has 25 000 nodes, 75 000 d.o.f. and 130 000 elements in 3D.

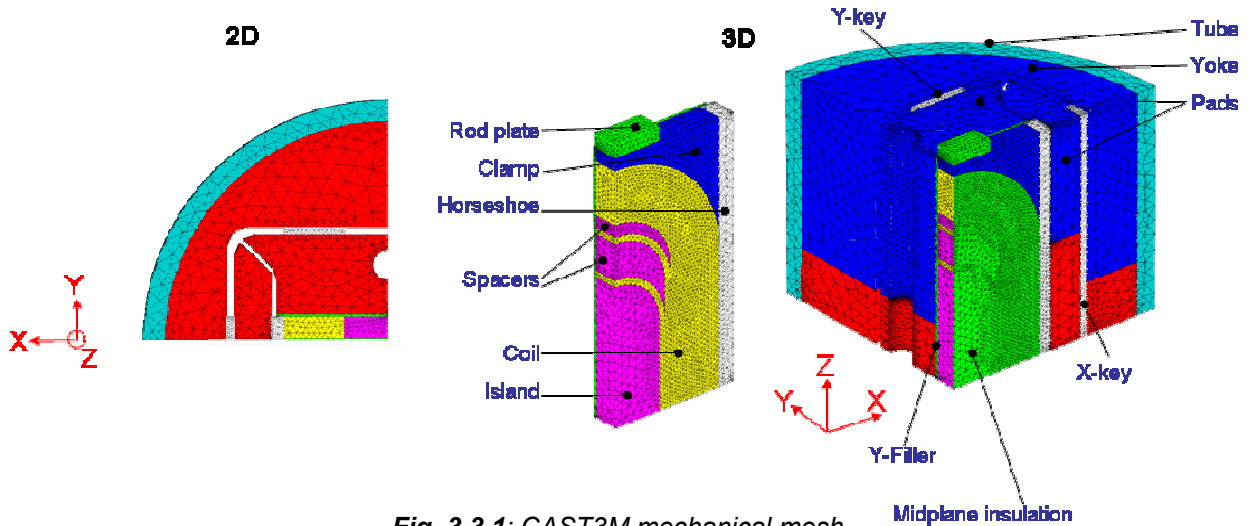


Fig. 3.3.1: CAST3M mechanical mesh

The assembly is modelled in one octant for symmetry reasons. As already explained, the double pancake coil is considered as one isotropic block (represented in yellow here). All the surrounding contacts are unilateral relations so that the conductor block can separate from titanium parts (in pink) and from the surrounding horseshoe (in white + blue). Identically, the support parts (tube, pads, yoke halves) are connected by unilateral relations allowing separation. Those contacts suppose no friction⁵. Picture 3.3.2 illustrates those contacts. Symmetry regions are represented in blue; glued planes are represented in pink; unilateral contact relations (without friction) are represented in green (uniaxial) and red (normal to the surface); the orange zone has no symmetry condition so that to simulate the yoke gap. The bladders interferences i_x and i_z are applied on the planes as showed.

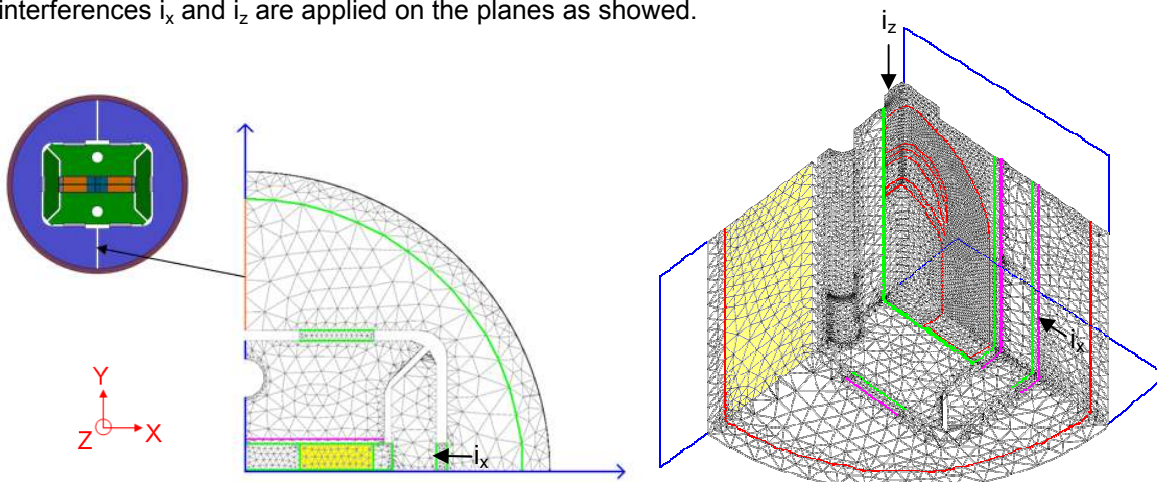


Fig. 3.3.2: boundary conditions and contacts in CAST3M

The model follows a six-step approach:



Fig. 3.3.3: mechanical computation diagram in CAST3M

⁵ Friction has been taken into account first. The conclusions remained almost unaffected by μ .

Geometries are updated after each step, material properties are refreshed for each level (room / cryogenic temperature). We first apply the horizontal bladder pre-stress at room temperature. We then skip to 4.2 K. The Lorentz forces are added gradually in order to take into account the nonlinear training along the current ramp. Anyway, the number of “loading” steps does not need to be larger. The 100%-case corresponds to the nominal 14 kA short sample forces, as presented in table 1.2.4. The 120%-case gives us a safety margin⁶.

The bladder shims and the longitudinal piston are not physically represented in this model. Their pre-stress is modelled in terms of interference between their support surfaces. This appears in CAST3M as a forced distance, kept constant during all steps (as if the preload keys were infinitely stiff). A 50 μm extra clearance should be taken into account for the shim insertion. This is not presented in this study. The corresponding water pressure can be indirectly evaluated by integrating the normal stresses on those surfaces:

$$P_{blad} \cdot L_{blad} = |\int \sigma_x(coil)| \cdot h_{coil} \quad (1)$$

The first computations are led in 2D in planar stress mode. The largest Lorentz forces occur in the {Z=0} plane, so this 2D pre-dimensioning is meaningful. This provides us with a baseline value for i_x , t_{shell} and r_{yoke} . The assembly behaviour is then controlled in partial and full 3D, with a longitudinal pre-stress i_z .

b. ANSYS™ [11]

This section and the following ones, dealing with the model results, are more extensively described in [12].

The 2D model consists in four-node elements “plane 42” within the plane stress mode (figure 3.3.4). The mesh used for the coil pack is identical to the magnetic mesh [6], so that the magnetic forces could be transferred using the ANSYS internal routine *LDREAD*. The mesh of the magnet pack and of the magnetic circuit (pads and yoke mainly) has been slightly revised, to reduce the simulation time. As previously stated, the materials have been considered fully isotropic (see table 3.1.1).

Since we are aiming to study the general behaviour of the magnet structure under the different lifecycle phases, and to define the on-plane reference preload value, the 2D model has been assumed frictionless.

As the stress deriving from the Lorentz forces is much higher along the horizontal direction, tending to separate the coil from the central post, we will focus on the definition of the lateral assembly interference i_x and how it can be combined with the shell and yoke thickness to provide a given pre-stress.

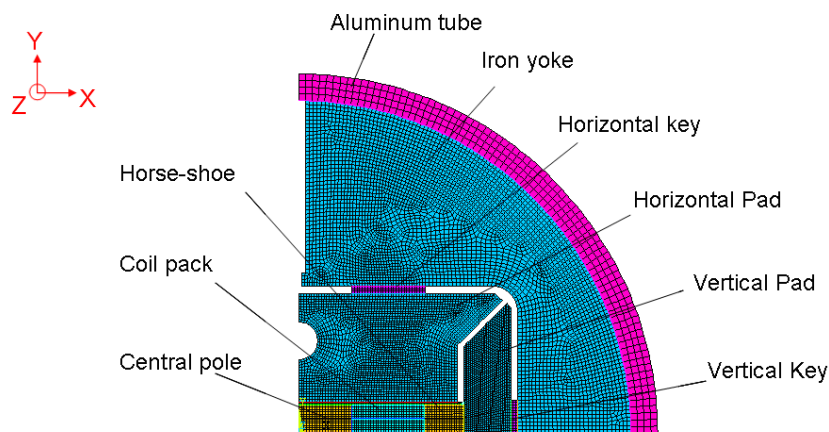


Fig. 3.3.4: ANSYS 2D mechanical mesh

The model consistency has been preliminary verified at room temperature (RT), by investigating the net compressive force between the outer coil profile and the related net tension force on the shell thickness. One can simply verify that:

$$\bar{\sigma}_{x,coil} \cdot h_{coil} = \bar{\sigma}_{r,shell} \cdot t_{shell} \quad (2)$$

First assessment analysis confirmed the validity of the equation (2).

⁶ Let's remark that to simulate current rising, we scale the force field rather than the current density field. This approximation enables us to avoid magnetic re-calculation at each step.

3.4- 2D Results

a. CAST3M

To get the orders of magnitude, we first evaluate every parameter's influence before magnetization. The influence of i_x ($0 \leq i_x \leq 500 \mu\text{m}$) on the lateral coil pressure is plot at room temperature (figure 3.4.1). It appears to be linear and almost equal on both sides. The influence of t_{shell} is plot after cool down. It is also almost equal on both coil sides but not linear. During both phases, the stress remains homogeneous on the coil.

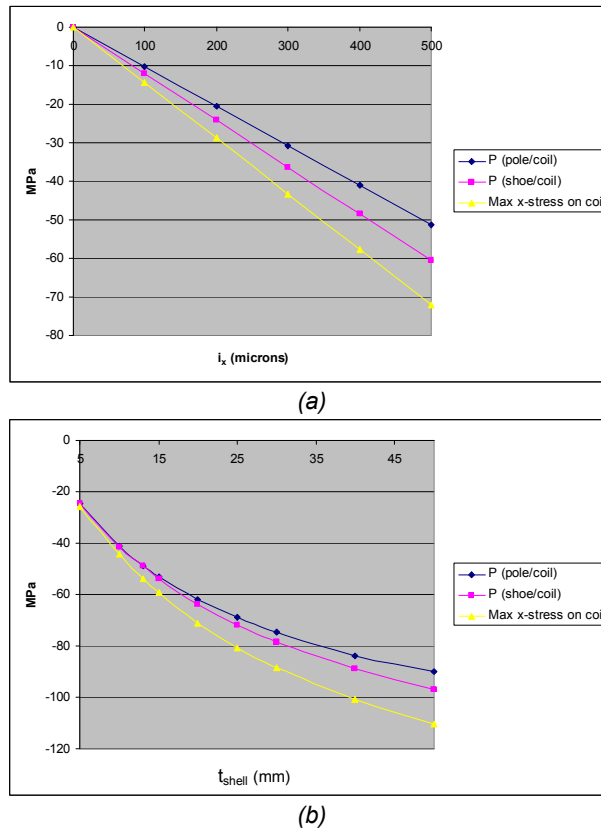


Fig. 3.4.1: i_x (a) and t_{shell} (b) influence on coil lateral pressure before magnetization

The Lorentz forces are then added (steps 3 to 5). They tend to “inflate” the double pancake as shown on figure 3.4.2: **the pressure increases on the shoe edge (by ~20 MPa) and decreases on the pole edge (by ~50 MPa)**. Thus, at short sample current, the coil tends to separate from the pole.

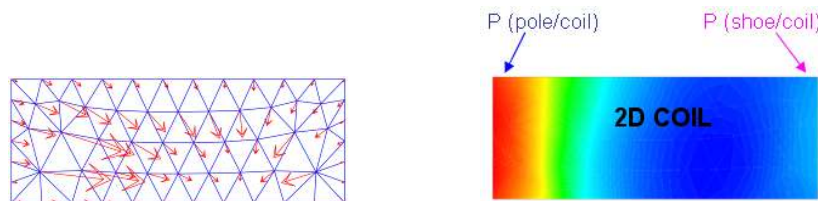


Fig. 3.4.2: Lorentz 2D nodal forces and resulting axial stress map allure

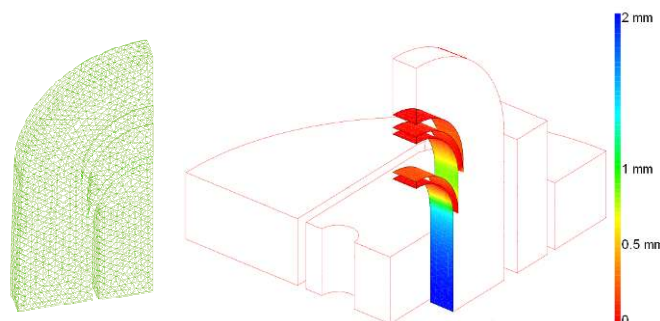


Fig. 3.4.3: visualisation of the coil/pole/spacers separations in a particular case ($i_x=0$)

The maximum stresses are observed inside the coil (around turn #15). To respect our specifications, we must compensate the separation effect by a sufficient pre-stress without exceeding the 150 MPa limit on the conductor. According to § 2.2, the best solution would be that the tube contraction compensates the Lorentz effect on the pole/coil separation, and that the bladders bring the variable remainder of the pre-stress. Many optimization rounds lead to choose $t_{shell} = 17-20$ mm and $i_x = 300-500 \mu m^7$. As we will point out later on, we finally decided to fix $t_{shell} = 20$ mm, leading to $i_x = 300 \mu m$, according to considerations made on analysis results. We evaluate $r_{yoke} \sim 220-250$ mm (see § 3.4.2).

Figure 3.4.2 shows the six-step lifecycle of the SMC magnet after 2D optimization in CAST3M with the following parameters: $t_{shell} = 20$ mm, $i_x = 300 \mu m$, $i_y = 0 \mu m$, $r_{yoke} = 230$ mm. For each step, the axial stresses on coil midplane and the Von Mises stresses on the structure are represented.

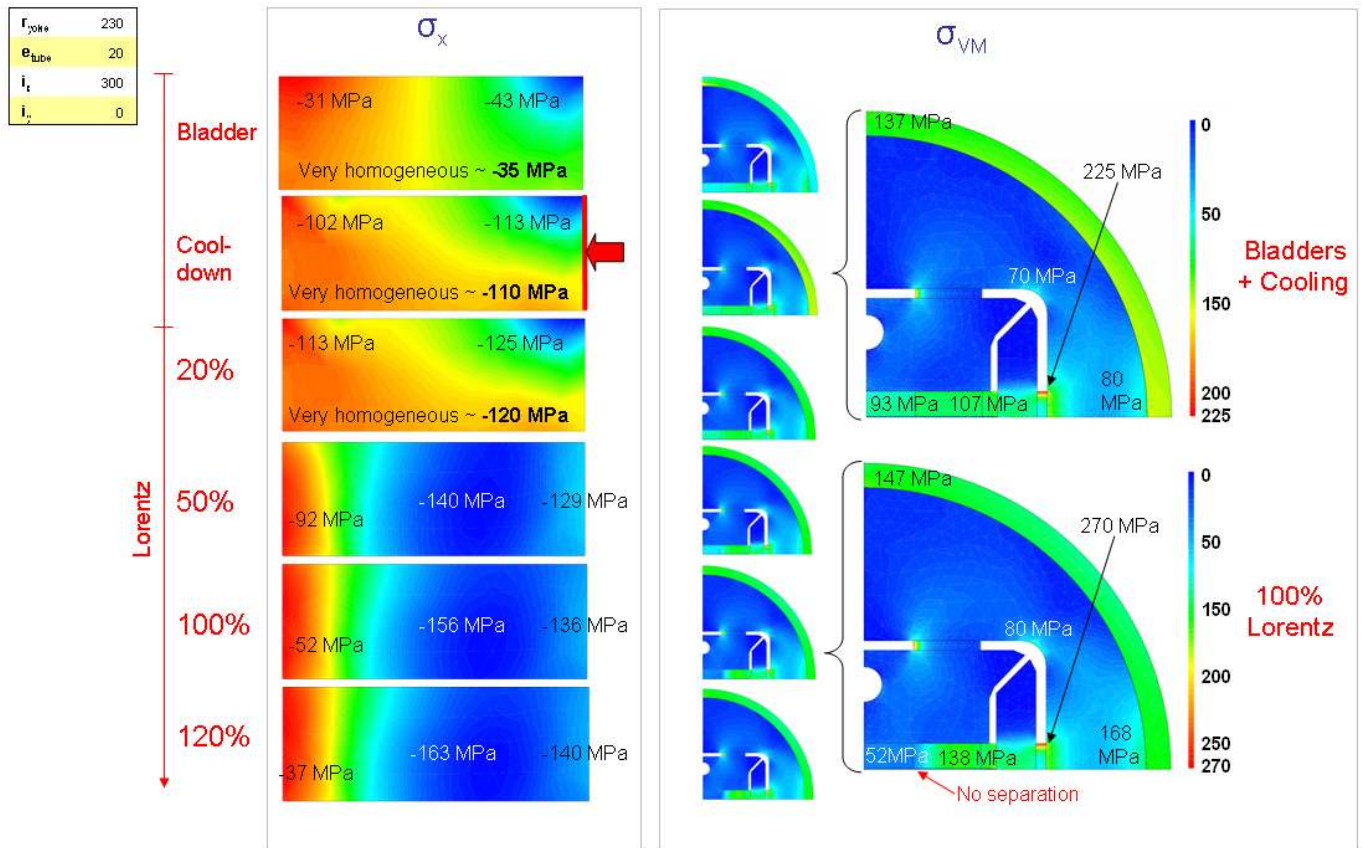


Fig. 3.4.4: SMC lifecycle after 2D optimization in CAST3M

In this 2D configuration:

- all parts remain safe during the process with high security coefficient ($\gg 2$)
- no separation occurs around the coil
- the stresses remain controlled on the conductor: $|\sigma_x| < 156$ MPa and $\sigma_{VM} < 138$ MPa.

We have the margin to be able to increase reasonably i_x . This is important for the mandatory bladders insertion clearance ($\approx 50 \mu m$). This configuration has been checked but is not represented here.

This configuration will be the starting point of the next 3D optimizations.

⁷ For comparison, the tube thickness was 13 mm in SD01. To get the same thermal pre-stress that SD01, we would need $t_{shell} = 25$ mm. For SMC, the bladders role is increased. This supposes to enhance them, as discussed in § 4.2.

b. ANSYS™

An analysis on the coil pre-stress during assembly, cool down, and powering has been carried out, by varying the lateral interference from 100 to 1000 μm , by steps of 200 μm (the shell thickness has been arbitrary set to 20 mm). The aim of this analysis is to check the maximum pre-load we can provide at warm, with a maximum stress on the coil around 150 MPa at powering. According to figure 3.4.5, the limit value for the assembly interference i_x is about 400 μm , with maximum Von Mises stress $\sigma_{VM,max} = 50$ MPa at warm, and ~ 155 MPa at short sample point.

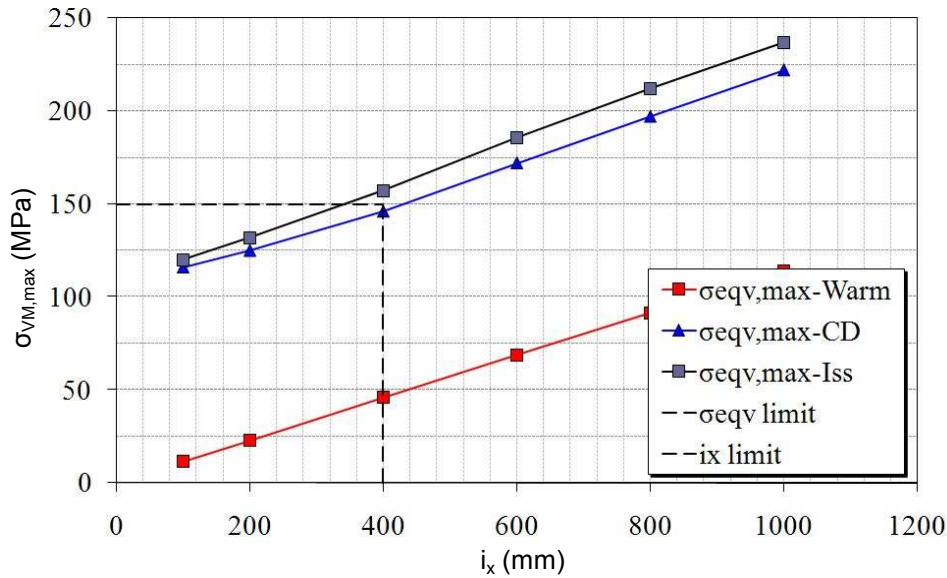


Fig. 3.4.5: $\sigma_{VM,max}$ as a function of i_x in ANSYS

The stress profile on the inner coil edge has been studied, in order to understand the stress transmitted to the G10 composite (glass fibre-reinforced epoxy resin) that impregnate the coil. This material can sustain a maximum traction load estimated around 20 MPa, beyond which the resin cracks and the coil separates from the titanium components. The analysis focuses on the powering phase, when the magnetic forces tend to separate the coil inner edge from the main post, loading at the same time the horseshoe side. It has been verified that the residual stress at powering is below 20 MPa.

As pointed out before, the coil preload derives from the combination of the assembly interference and the shell thickness. We now want to analyze how these parameters can combine to provide a target pre-stress, and how the yoke radius r_{yoke} influences it.

The influence of the yoke thickness on t_{shell} has been investigated for a given set of assembly interferences, by imposing the following design criteria:

- the residual stress between the coil and the main post $\bar{\sigma}_{x,cp}$ has to be lower than 20 MPa;
 - $\sigma_{VM,max}$ on the coil must be below 150 MPa;
 - the failure criteria for the dipole components have to be observed by means of a safety factor equal to 1.5.
- The Von Mises criterion has been selected for ductile materials at both warm and cold temperatures, apart for the magnetic items, made from low carbon MAGNETIL steel, experiencing brittle fracture at cryogenic temperature. The failure criterion that has been used for them is the Rankine's: the first principal stress is responsible for the component collapse, and has to be compared to the UTS (Ultimate Tensile Strength).

This analysis (see figure 3.4.6) shows that an increase in yoke thickness up to 55 mm leads to higher pre-stress at warm, due to the augmented system rigidity, so that a thinner shell can be used. For thicker yoke widths, the preload is then completely determined by the shell and keys dimensions. For a given pre-stress, a bigger interference increases the pre-load at warm thus implying a thinner aluminium shell. The curves represent the boundary between: (i) an insufficiently loaded system, involving the risk of coil detachment from the main post, and (ii) an over-loaded system, where the equivalent stress provided to the coil is higher than 150 MPa. For a given magnet configuration, it will be anyway possible to play around the curve with the shims, in order to decrease or increase the coil pre-stress, avoiding premature quenches due to coil movement.

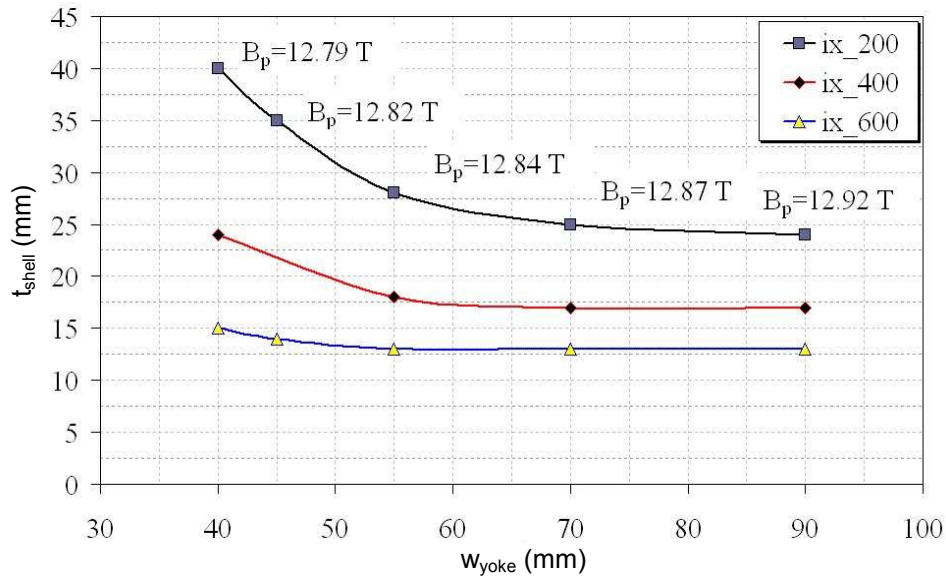


Fig. 3.4.6: t_{shell} as a function of w_{yoke} ⁸ in ANSYS with the above-mentioned criteria [B_p represents the peak field on coil]

The final values of the shell thickness and the yoke radius have been set to **20 mm** and **230 mm** ($w_{yoke}=90$ mm) respectively. This choice has been driven by several reasons: the commercial shell thicknesses available, the need for a reduced outer field (0.6 T here), the availability of stock laminations for the iron parts, and the cryostat inner diameter. Finally, due to the combination of these two parameters, the key assembly interference i_x is set to **300 μ m**.

⁸ The yoke thickness is directly correlated to the yoke radius: $w_{yoke} = r_{yoke} - 140$ mm

3.5- Simplified 3D results with CAST3M

Before implementing the full 3D model, we have set up a simpler 3D model with only the coil pack. As in 2D, the mesh is imported from the magnetic optimization phase. We take into account a limited number of parts: island, spacers, coil, rod plate, horseshoe and its clamp (as defined in figure 3.3.1). The contacts are set as showed in figure 3.3.2. The influence of the surrounding parts (pads, bladders, yoke, tube) before magnetization is implemented in terms of a lateral pressure in the X direction, applied to the coil pack lateral edge as showed on picture 3.5.1. The value of 113 MPa is taken from the 2D model, step 2 as showed in figure 3.4.4. The nodal Lorentz forces are added then. The horseshoe can be split into two parts by applying a sliding contact between blue and white parts.

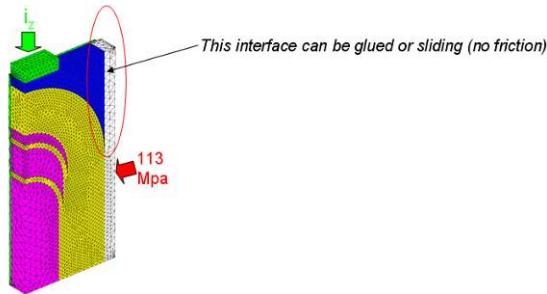


Fig. 3.5.1: coil pack 3D modelling

This model should answer three questions:

1. What would happen without longitudinal support ($i_z=0$)?
2. How does i_z affect the 2D mid-plane results?
3. Is it better to have a full-block horseshoe or to divide it into four separated parts?

The answer to the first question is illustrated on picture 3.5.2: without longitudinal support, large gaps tend to open along the spacers. This causes torsion to the coil leading to very high stresses on the conductor. **A longitudinal support is mandatory.**

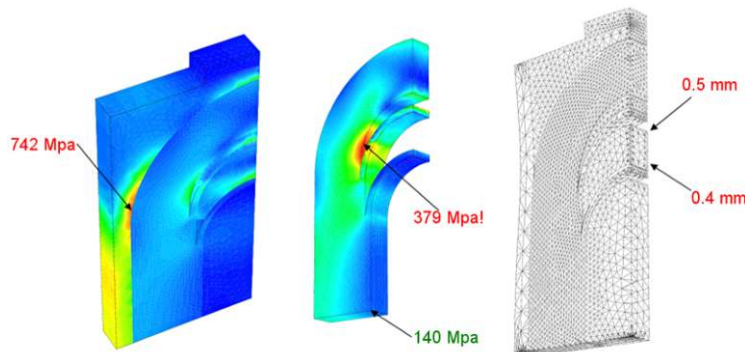


Fig. 3.5.2: coil pack behaviour at 14 kA without longitudinal support

About the second question, calculations show that the coil pack mid-plane behaviour is not too much affected by the longitudinal pre-stress (table 3.5.3). It is practically important because it enables us to transpose the 2D optimization results in the 3D case, and to offset only i_z .

	i_z (μm)	$\sigma_x(\text{pole})$ (MPa)	$\sigma_x(\text{shoe})$ (MPa)
2D	/	-37	-140
3D	0	-29	-137
	250	-31	-137
	500	-32	-138
	750	-33	-138
	1000	-35	-139

Tab. 3.5.3: radial stresses on coil edges in 2D and in simplified 3D for different i_z

About the third question, we observe very little difference between the configurations. Both solutions are equivalent in terms of stress repartition⁹. A full-block horseshoe will be thoughtfully preferred for realization.

⁹ This study is secondary: no precise results are given here. Nevertheless, a detailed feedback can be found in [13]

3.6- 3D results with CAST3M

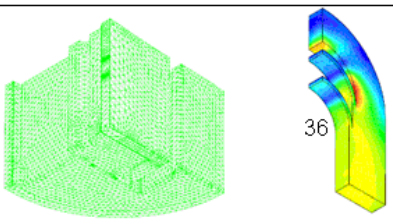
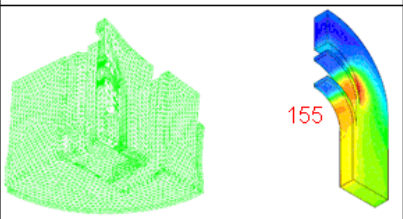
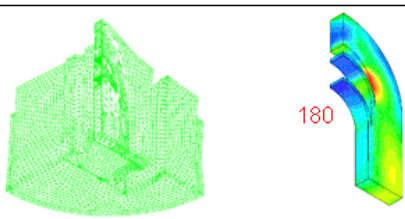
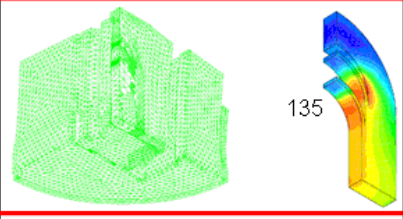
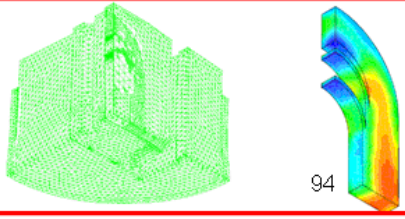
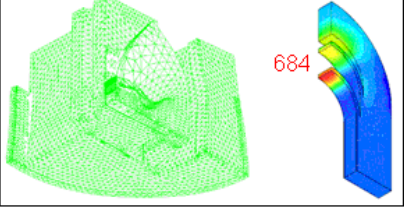
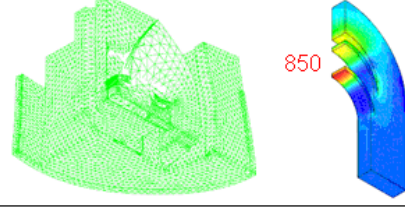
Paragraphs 3.4 and 3.5 have given the optimized values for t_{shell} and i_x and an order of magnitude for r_{yoke} . We have also seen that skipping to 3D does not dramatically affect the 2D conclusions and that a longitudinal support is mandatory. On that base, the idea of the 3D model is:

- to define the appropriate longitudinal pre-stress
- to verify the respect of the specifications everywhere in every part during the magnet lifecycle.

a. Coil behaviour analysis

In real life, the longitudinal pre-stress is applied by the rods thermal compression plus an additional piston pressure. The rods optimization will be performed with ANSYS. CAST3M model gathers both effects in a single interference i_z . This simplification aims at proving that it is possible to find a value for i_z such that the stresses are well-controlled in the structure.

The development of the full 3D model has been long and only final results will be presented here. This model is based on the 2D optimized values. Next plots summarize the 3D results in three cases: $i_z=500$ or $2000 \mu m$ or "no i_z " (i.e. no support). Obviously, many other possibilities have been tested. Table 3.6.1 shows the structure deformations (x100) and the coil equivalent stresses during cool-down and at 14 kA. The intermediary magnetization steps have been hidden. The pre-stress step is only presented without support because the way we apply i_z does not correspond to reality: corresponding results would be misleading. In reality the longitudinal pre-stress will not be applied at once (as it is here): the rods will contract progressively during cool-down, following the other parts' deformation.

	PRE-STRESS (room temp.)	COOL-DOWN	I_{ss}
no rod (free)			
$i_z=500$			
$i_z=2000$			

Tab. 3.6.1: structure deformation (x100) and Von Mises coil stresses (MPa) for different i_z (CAST3M)

Without any support (case 1), the coil stresses remain low after pre-stress (<36 MPa) but they reach 180 MPa at I_{ss} on turn #5: this could reduce significantly the magnet performances at nominal current.

A too large i_z neither appears good: it clamps the conductor in the end, causing very high stresses (up to 500 MPa with $i_z=1000 \mu m$ or 900 MPa with $i_z=2000 \mu m$).

When $i_z=500 \mu m$, the situation seems safe. The peak Von Mises stress at I_{ss} is below 100 MPa. This is 40% lower than in the 2D case (138 MPa) showing that in spite of our § 3.5 comment, the longitudinal effect *does* affect the median plane results. But this simplification has made our optimization more efficient. In this configuration, the structure shape appears to be less distorted. This means that the longitudinal effect has just been set to compensate the thermal compression plus the Lorentz forces and the bladders effect. This preliminary study needs to be completed, particularly for first step: this will be done with ANSYS in § 3.7.

b. Structure analysis

We have showed that a safe configuration in terms of coil stress management exists. We now need to check if this configuration suits to every structural part. Table 3.6.2 shows the relevant indicators for successive steps (bladders pre-stress, cool-down, 100% and 120% of Lorentz forces) with $i_z=500 \mu\text{m}$. Once again, the coil equivalent stresses and deformation are not represented at room temperature because of the longitudinal modelling. However plots are given for the other structural parts which are not or much less affected by i_z but by i_x . Iron is brittle at cryogenic temperature, so we should also compare its principal stress with its UTS during steps 2 to 6. This is not done here (see § 3.7). Nevertheless we are far enough from the criterion limits so that we can confirm that the situation is safe in the iron.

After pre-stress (step 1), contact is maintained around the coil. The stresses are under control everywhere in the support structure.

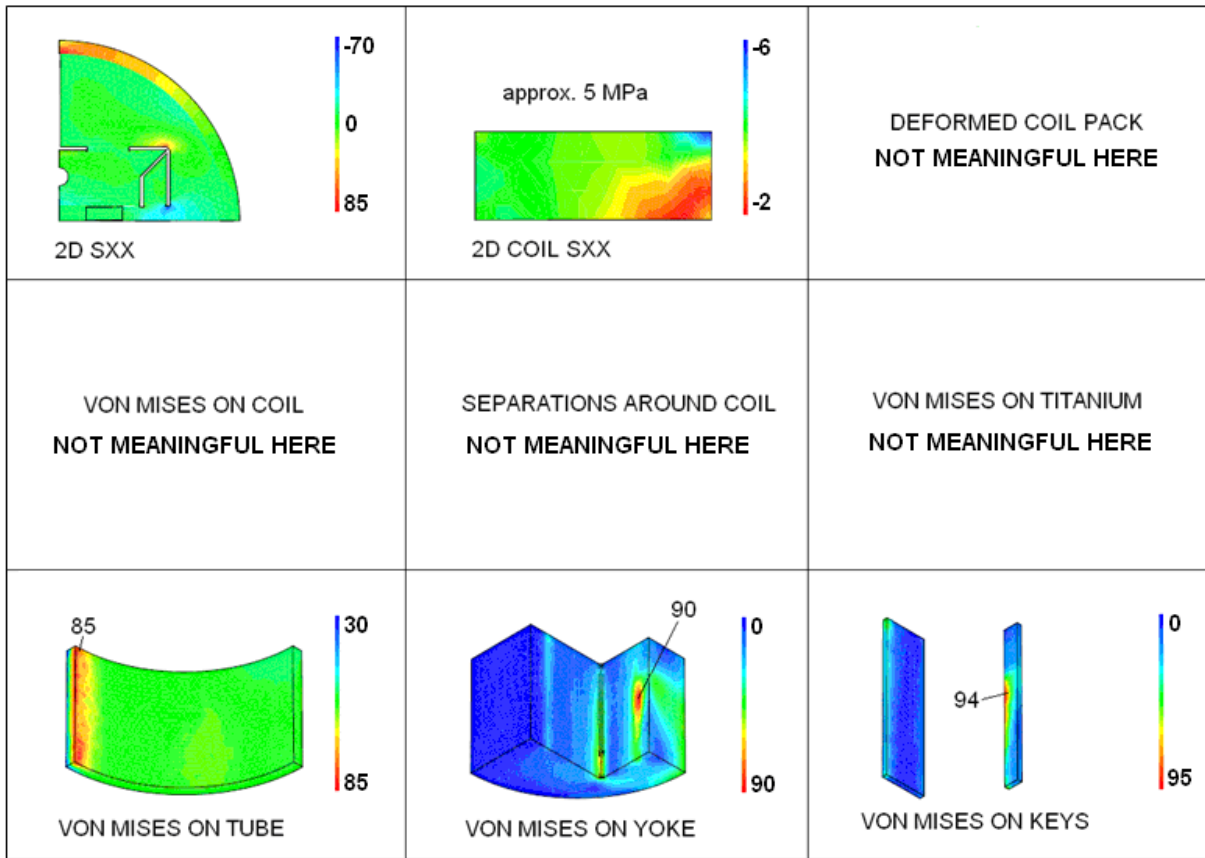
After cool-down (step 2), the coil stresses remain below 135 MPa. The contact is maintained around coil and the stresses are controlled everywhere. We can point a peak at 320 MPa on the Y-keys. The outer tube that brings the pre-stress remains under 140 MPa.

At short sample current (step 5), the coil stresses remain below 140 MPa. The contact is maintained around coil (the 40 microns separation is a calculation residue) and the stresses are controlled everywhere. This is a very efficient configuration.

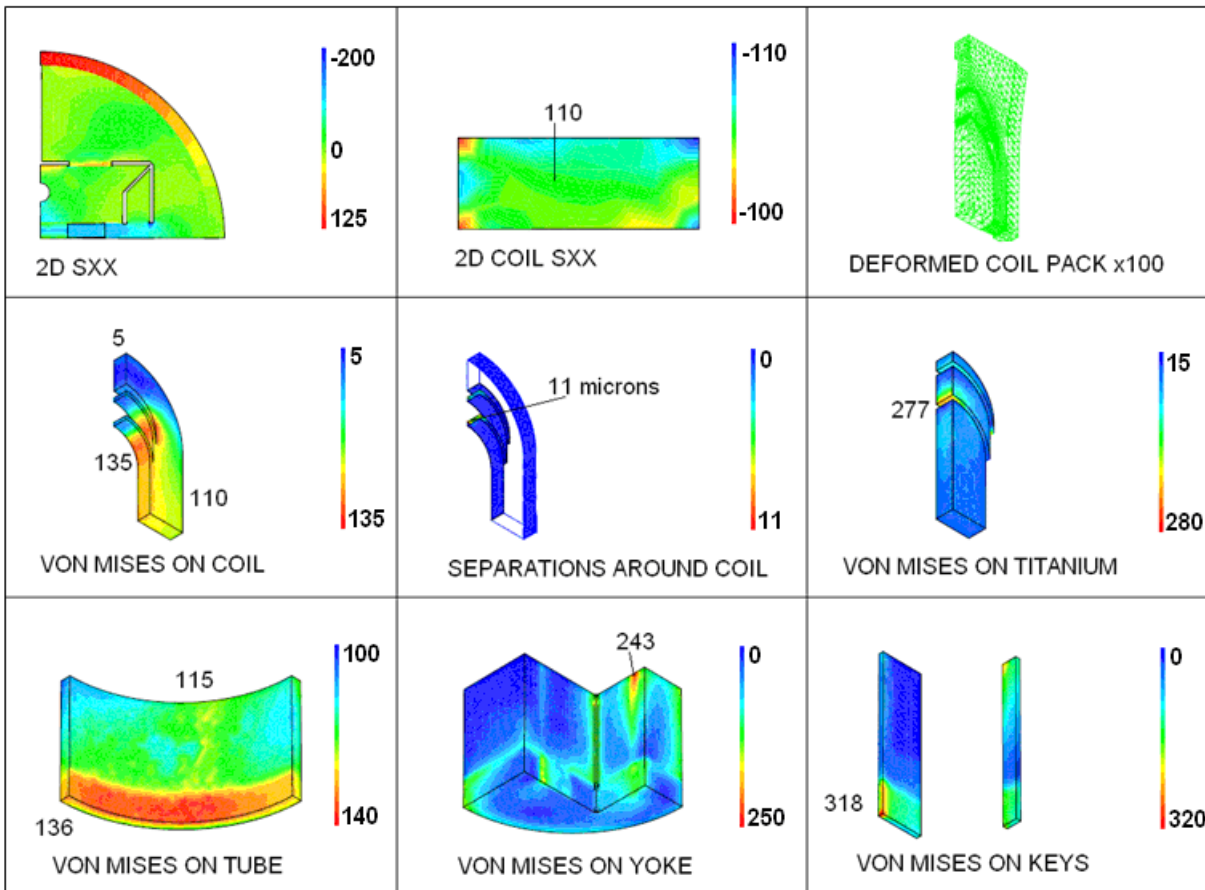
Those results are confirmed at 120% I_{ss} (step 6).

This study shows that a configuration for which the magnet and the structure are safe after cool down and powering exists. The rods dimensioning will be done in ANSYS, in order to set the correct longitudinal pre-load to provide by means of the hydraulic jack and rods.

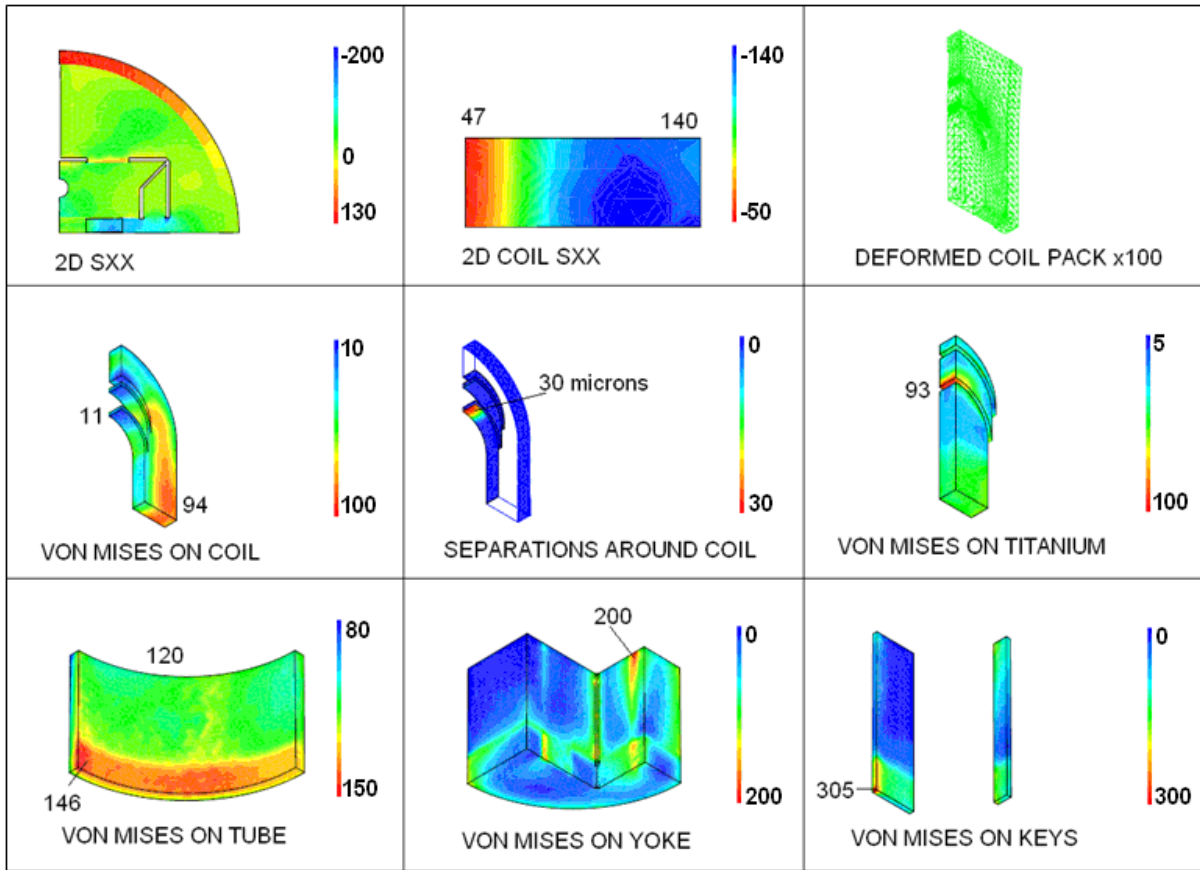
Step 1: PRE-STRESS (room temperature)



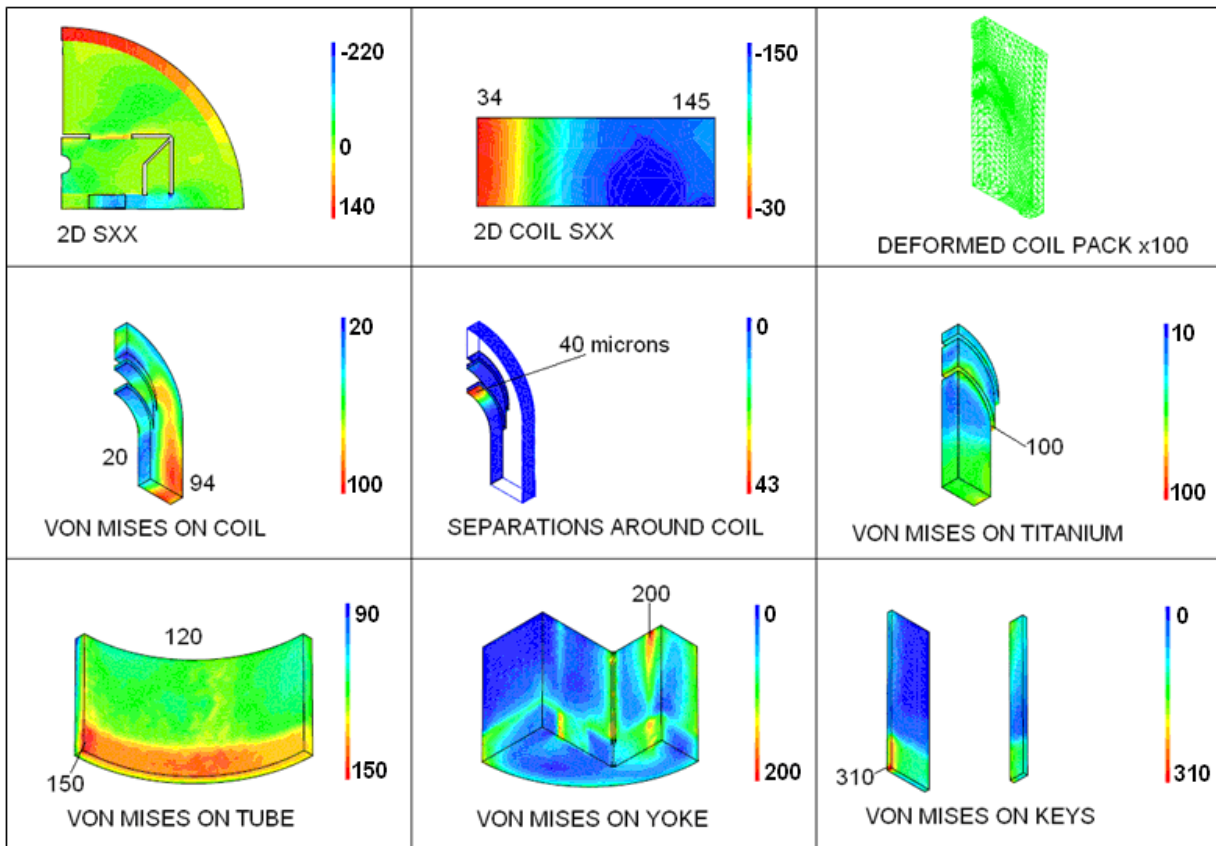
Step 2: COOL-DOWN (2 K)



Step 5: 100% I_{ss} (nominal case, 14 kA)



Step 6: 120% I_{ss} (conception margin, 16.8 kA)



Tab. 3.6.2: optimized structure lifecycle (CAST3M)
[stresses in MPa; displacements in μm]

3.7- 3D results with ANSYS

a. Model description

The aim of the ANSYS 3D model is firstly to set up the longitudinal pre-load in order to keep the cables in contact with the titanium components (island and spacers), under the action of the magnetic forces. The pre-load system will be designed and consequently dimensioned. Secondly, a complete analysis on the coil stress distribution as well as on the magnet items will be performed, during: (1) assembly, (2) cool down, and (3) powering at critical current.

The 3D model has been realized in ANSYS on the base of the magnetic one, implementing the outer shell and the longitudinal pre-load system (figure 3.7.1). Only 1/8th of the model has been defined for symmetry reasons in the space domain $\{O_x \geq 0, O_y \geq 0, O_z \geq 0\}$.

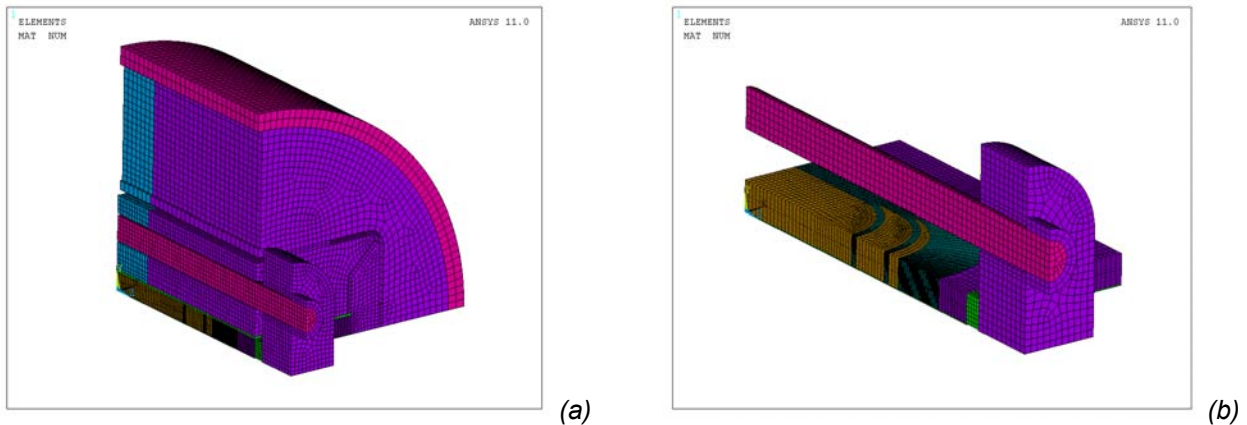


Fig. 3.7.1: ANSYS 3D mechanical model: (a) entire model, (b) longitudinal pre-load system

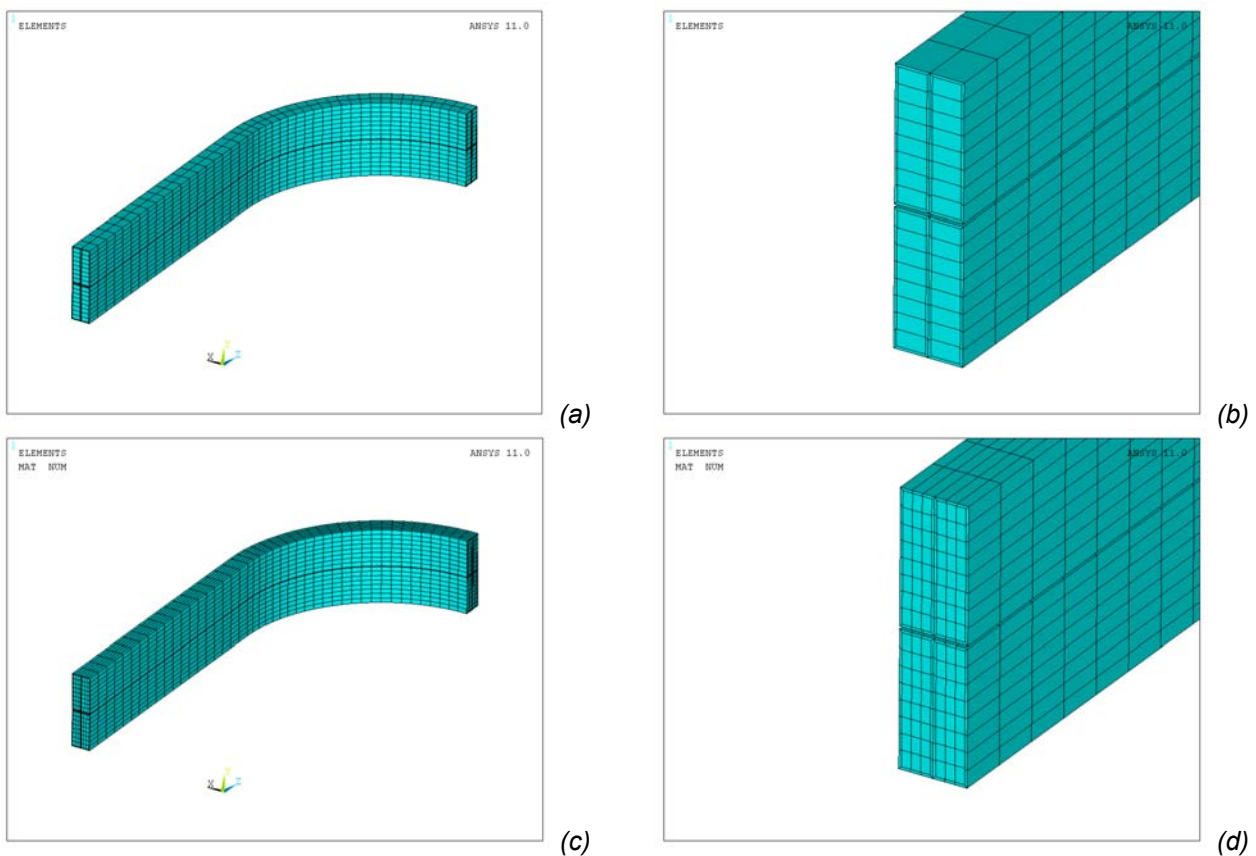


Fig. 3.7.2: conductor meshes in ANSYS for the magnetic model (a-b) and the mechanical one (c-d)

The coil is the only part affected by major mesh changes; numerical imprecision due to the highest aspect ratio between the insulation and the bare cable elements have been observed adopting the same mesh than the magnetic model. After some refinements, the bar cable width has been finally divided into three elements (0.7 mm-width) instead of one (2.1 mm).

As outlined before, the coil is impregnated by a glass fibre epoxy-reinforced composite and substantially glued to the containing structure after impregnation. For stress higher than 20 MPa (in tension) the impregnation can break, allowing cable movements. There are two ways of defining the characteristics of the contact elements between the winding and the coil items: either (1) considering the contact area as fully bonded (linear analysis) and checking the local stress with respect to the assumed limit, or (2) considering friction contact with sliding and separation allowed, since the coil could actually separate from the inner pole and spacers, if the stress is too high.

None of the two approach can be considered fully exact, since it should be introduced a control on the maximum stress on the G10 at every simulation step. We have anyway opted for the first solution, since it can be considered as the closest to the real configuration of a glued assembly.

The contact elements used elsewhere in the model have been considered frictionless, in order to have a general picture of the system behaviour. This can be considered as a preliminary model set-up; later modifications and improvements on contact status will be introduced once the magnet will be tested. In particular, the friction coefficients will be tuned on the base of the state of the art on material tribology and on the magnet experimental results.

Since the magnetic and mechanical meshes do not coincide, it will not be possible to use the LDREAD command to transfer the magnetic forces to the mechanical model. We will use an *ad-hoc* routine realized in ANSYS in order to store the forces from the magnetic model and to transfer them to the mechanical one using nodal coordinates [6,12].

b. Parametric analysis of the longitudinal pre-load

The system used in SD01 to exert the longitudinal pre-load is represented in figure 3.7.1. This system has been successfully used in magnets previously realized at LBNL. It consists of two aluminium rods running through the magnet pack from one extremity to the other, bolted on two stainless steel end-plates which transfer the load to the coil pack.

At warm, the rods are put in tension by means of an hydraulic jack placed at one end, and then fixed in place at the jack side by means of a couple of nuts. By acting on the jack pressure and on the nuts is so possible to set-up the required pre-load level, accordingly to the user needs. The total coil pre-stress is then achieved at cryogenic temperature by exploiting the differential thermal contraction between the rods and the coil pack. For this analysis, we assume a rod diameter of 28 mm. The aluminium alloy is the same as for the outer shell (Al 2014 T651).

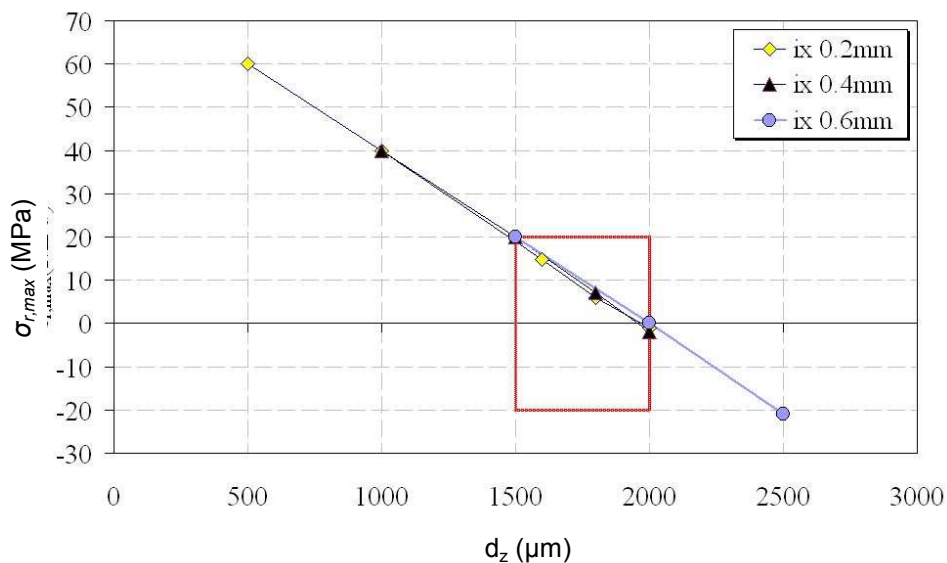


Fig. 3.7.3: $\sigma_{r,max}$ on the inner coil head as a function of the longitudinal pre-load displacement d_z for different lateral assembly interferences (ANSYS)

The coil longitudinal pre-stress must be set up in relation to the maximum stress at the boundary between the coil and the titanium components, namely the radial stress σ_r accordingly to the local cylindrical coordinate system. Since the highest stress level occurs between the first cable and the main post, this will be assumed as our reference value in order to define the correct longitudinal load. This parameter will be expressed in terms of rod displacement d_z (μm) at $z=0$. The results of the parametric analysis are represented in figure 3.7.3. Three different lateral interferences have been set ($i_x=200, 400, 600 \mu\text{m}$) whereas the longitudinal displacement ranges from 1000 to 2500 μm . It can be seen that the minimum displacement we have to provide the structure is about 1.5 mm, to have $\sigma_r \leq 20 \text{ MPa}$, independently from the lateral interference. This is due to the invariance of the lateral pre-load achieved, since the shell thickness has been changed for a given assembly interference according to the results shown in figure 3.4.6.

The net magnetic longitudinal force in SD01 was about 85 kN for each pancake; the longitudinal rod displacement d_z^{SD01} was set to 380 μm . The total magnetic force has been estimated around 260 kN for the SMC; by scaling on the magnetic forces, the expected $d_z^{\text{SMC}} \sim 1200 \mu\text{m}$. This first guess value is so consistent with the results described before.

c. Final configuration

The final configuration of the SMC slightly differs from the one reported in [6]. It has been decided to use massive stainless steel lateral pads, since their influence on the magnetic field pattern is secondary (see § 4.1.b). In this way we are able to provide a more uniform stress along the coil side. The shape of these pads has been reviewed as well in order to accommodate different coils into the magnet aperture; in particular it has been envisaged the possibility of testing the SMC optimized coils with innovative ceramic insulation developed at CEA. Being this insulation thicker, a bigger aperture is so required.

We will now describe the stress analysis on the final configuration, whose parameters are listed in table 3.7.4. The analysis results are summarized in table 3.7.8.

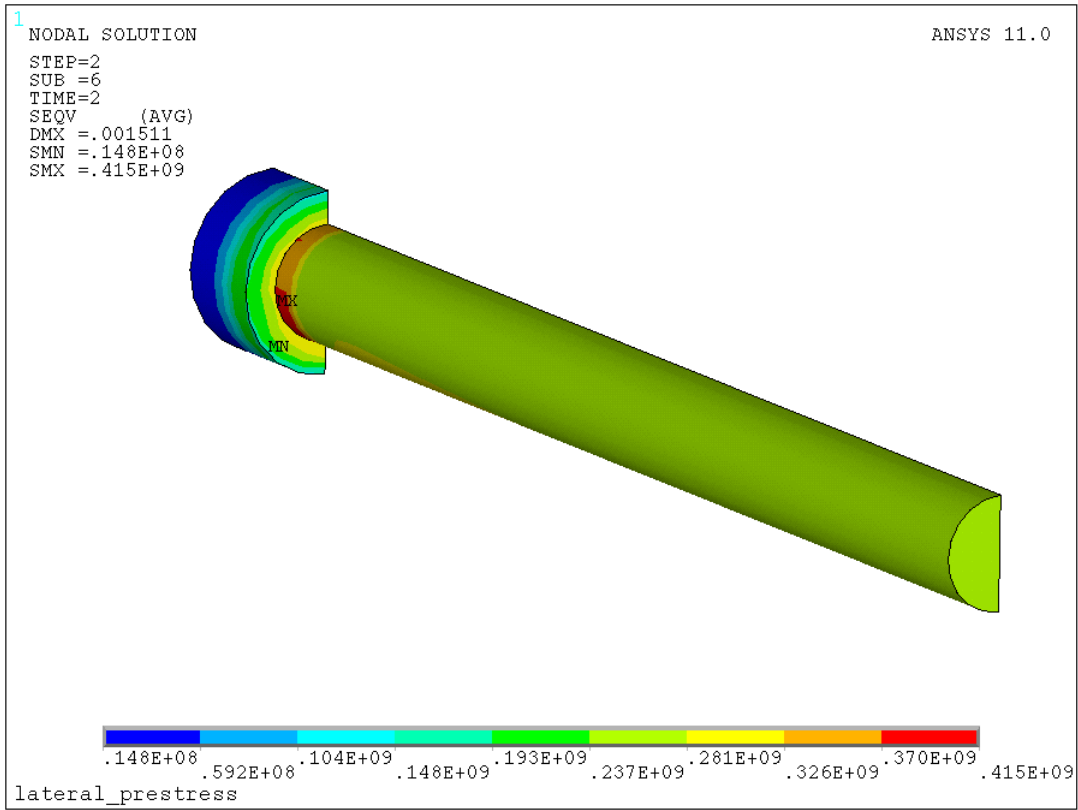
Parameter	Name	Unit	Value
Shell thickness	t_{shell}	mm	20
Assembly interference	i_x	μm	300
Rod diameter	\varnothing_{rod}	mm	30
Rod displacement	d_z	mm	1500

Tab. 3.7.4: 3D assembly and pre-load parameters (ANSYS)

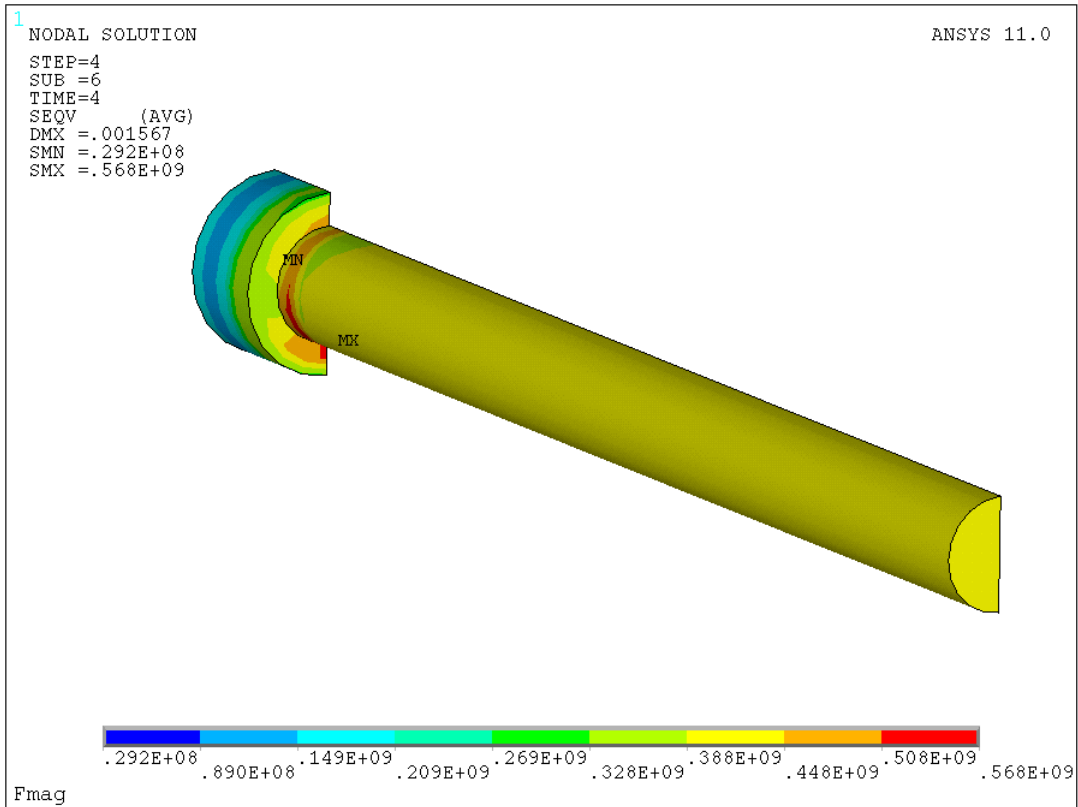
By loading the rods by means of the hydraulic jack, a compressive state on the coil heads is achieved. On the other hand, the rods are under general tension. The longitudinal compressive stress on the coil $\sigma_{z,coil}$ increases from the coil straight section towards the heads due to the rod effect. By looking at the coil heads locally (see figure 3.7.6.a), this aspect is more evident: the maximum radial stress occurs at the Ox symmetry plane, whilst decreasing towards the straight section. This trend is more evident in the outer pack, where σ_r decreases from 60 MPa (compression) to 8 MPa (tension).

By applying the lateral interference, with 300 μm thick shims, the lateral stress along the coil straight section is about 30 MPa in compression. It can be easily derived the minimum bladder pressure corresponding to this stress level, scaling on the coil and bladder width. This value is about 127 MPa. Nevertheless, an overload will be required in order to get enough clearance to slide the shimmed keys inside the magnet pack ($\sim 100 \mu\text{m}$). The coil heads undergo a generalized state of compression, ranging in $[-0; 60] \text{ MPa}$.

The residual stress between the winding straight section and the main post is negligible. The rods show a localized maximum point of about 400 MPa in correspondence of the nut (see fig. 3.7.5); nevertheless this point can be considered as a singularity due to the contact element behaviour between two different materials. Due to the uniformity of the stress distribution along the rod body, we can conclude by neglecting this singularity, and consider the Von Mises criterion as fulfilled with a security factor of 1.5.



(a)



(b)

Fig. 3.7.5: σ_{VM} in the longitudinal rods after (a) assembly and (b) powering (ANSYS)

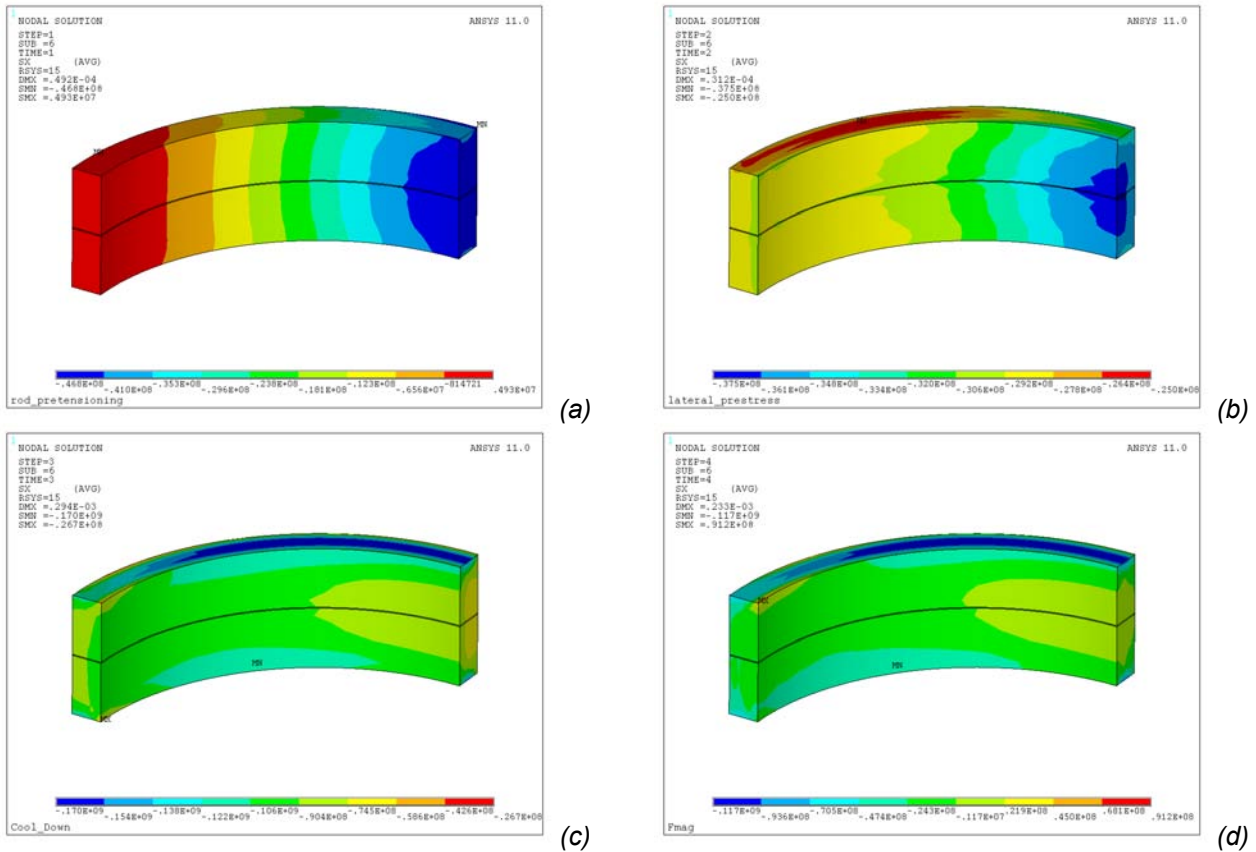
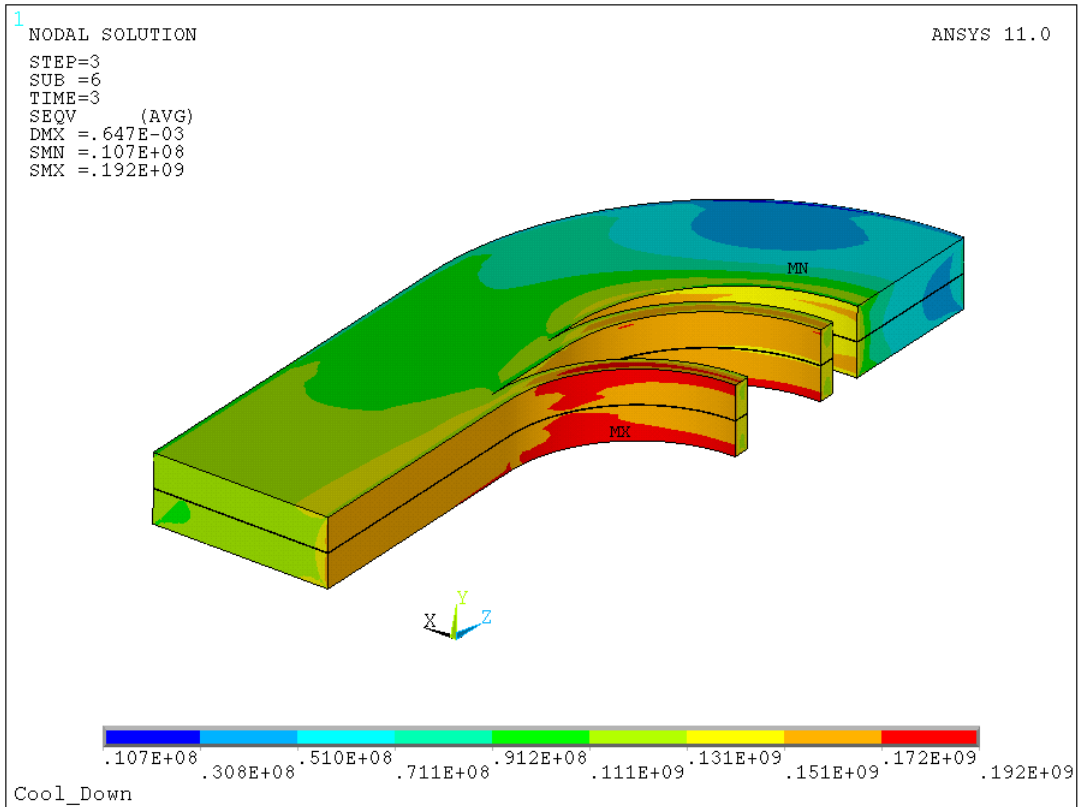


Fig. 3.7.6: σ_r evolution in the inner coil head after (a) longitudinal pre-load, (b) lateral pre-load, (c) cool down and (d) powering (ANSYS)

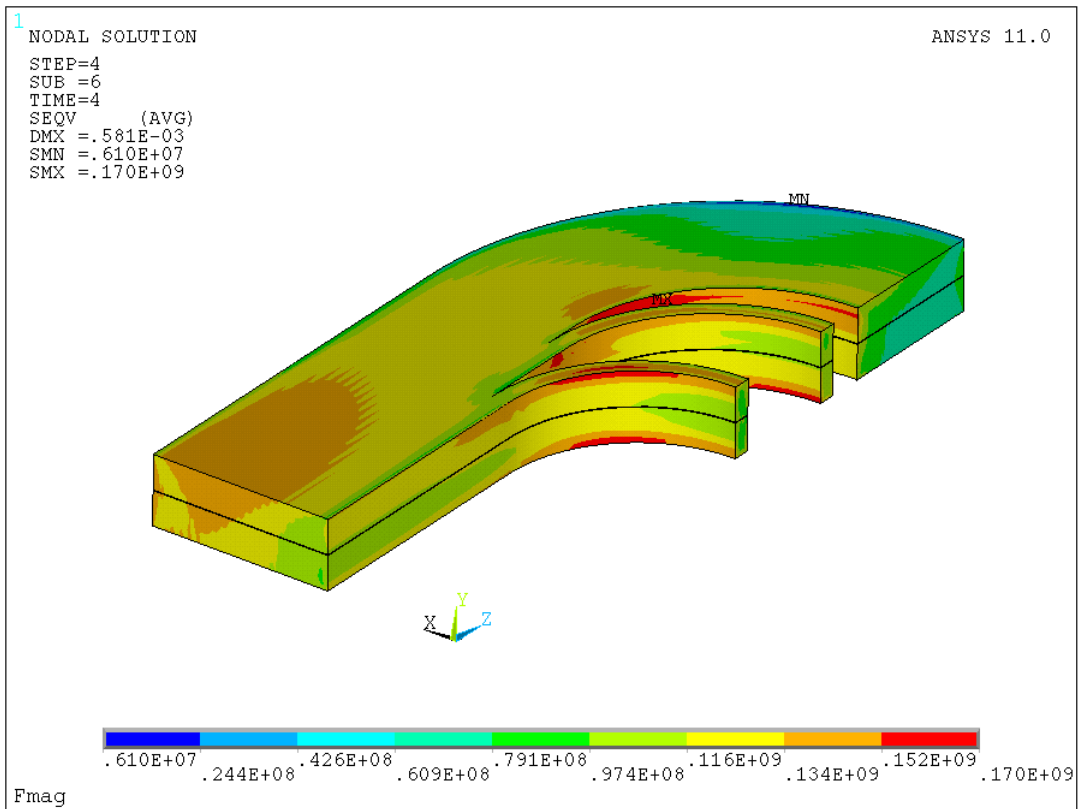
The gain in azimuthal stress σ_θ in the shell after cool down is about 80 MPa, which is consistent with the value of about 100 MPa, experienced in LBNL magnets. By scaling the incremental stress at cool down on the coil pack, we expect a gain in the lateral stress on the coil of about 75 MPa, leading to a total value of 100 MPa, confirmed by the numerical results. Due to the reduced thermal contraction of titanium alloy, the coil heads undergo a tension stress state along the bending radius, whereas the radial stress increases up to 150 MPa due to the effect induced by the aluminium rods.

After powering, the stress σ_x along the pole-coil side decreases from 110 MPa down to 30 MPa, due to the effect of the Lorentz forces. After cool down, we have noticed a maximum equivalent stress $\sigma_{VM,max}$ of about 190 MPa (see figure 3.7.7.a) at the boundary between the first lower cable head and the main post. Nevertheless, the magnetic forces arising during powering help redistributing the stress, lowering down to a maximum of 150 MPa (see fig. 3.7.6.b), as our design criteria impose. The equivalent stress in the aluminium components does not change, revealing that the pre-load parameters can perfectly balance the magnetic forces preventing from separation at the coil-pole boundary. All the steel components fulfil the related failure criteria; no particular issues on the titanium components are observable.

The minimum radial compressive stress on the first coil head is about 0 MPa (see fig. 3.7.6.d), rising to a maximum of 100 MPa on the outer head. Moreover, the stress pattern on the outer shell as well as on the rods does not change from cool down to powering, revealing that the action of the magnetic forces is counterbalanced by a proper system pre-load. This configuration could reasonably lead to the test of the SMC without leading to quenches due to cable movements. It will be anyway mandatory to perform preliminary test on the SMC structure to verify the FE model by means of a dummy coil (e.g. aluminium alloy), and eventually to feed back into the coil model to set up properly the contact elements behaviour.



(a)



(b)

Fig. 3.7.7: σ_{VM} in the coil pack after (a) cool down and (b) powering (ANSYS)

Item	σ (MPa)	Axial pre-load	Lateral pre-load	Cool down	Powering
Coil	$\sigma_{VM,max}$	57	38	193	130
<i>Nb₃Sn limit</i>	σ_{lim}	150	150	150	150
Shell	$\sigma_{VM,max}$	6	60	140	140
Rod	$\sigma_{VM,max}$	270	280	430	430
<i>Al 2014 limit</i>	σ_{lim}	415	415	545	545
Y-Pad, Yoke	σ_{max}	7	35	130*	130*
<i>MAGNETIL limit</i>	σ_{lim}	180	180	723	723
Pads, Yoke	$\sigma_{VM,max}$	14	45	160	160
Horseshoe	$\sigma_{VM,max}$	140	160	370	300
End plate	$\sigma_{VM,max}$	306	316	470	491
Vertical key	$\sigma_{VM,max}$	20	100	370	300
<i>AISI 316 LN limit</i>	σ_{lim}	350	350	1050	1050
Main post	$\sigma_{VM,max}$	40	40	15	140
first spacer	$\sigma_{VM,max}$	70	44	227	300
second spacer	$\sigma_{VM,max}$	80	46	227	300
<i>Ti6Al4V limit</i>	σ_{lim}	890	890	1700	1700

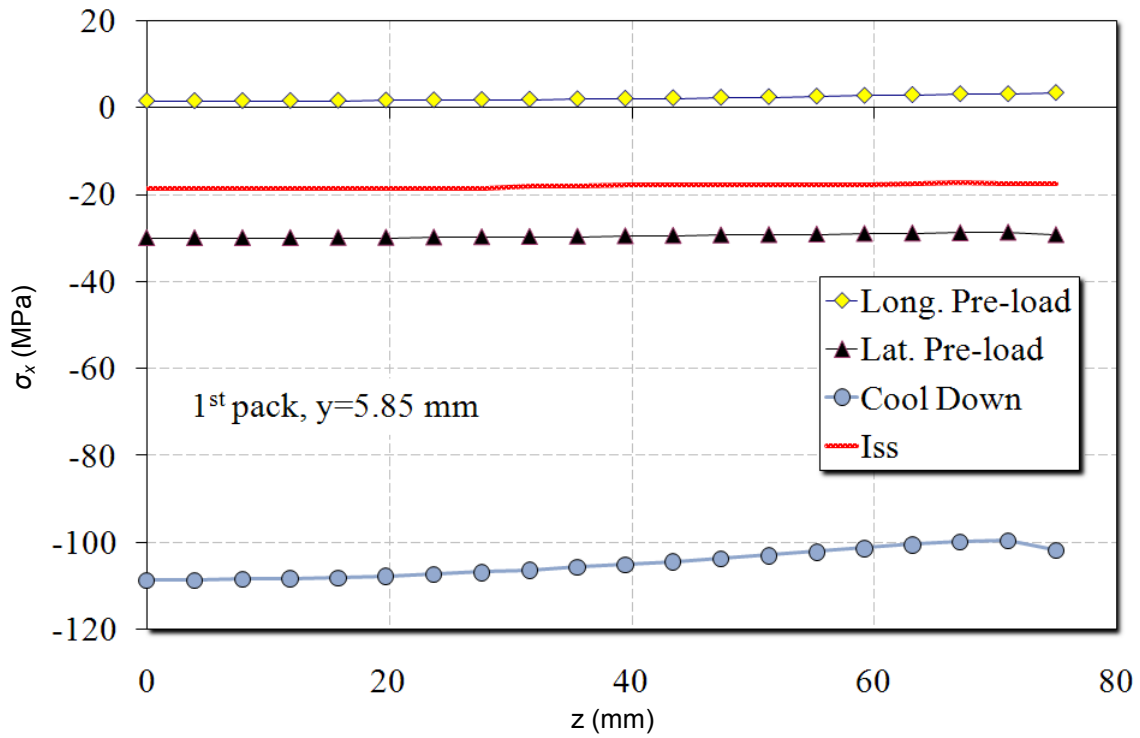
Tab. 3.7.8: SMC 3D model results in ANSYS

**the maximum stress for the MAGNETIL items after cool down and powering is the first principal*

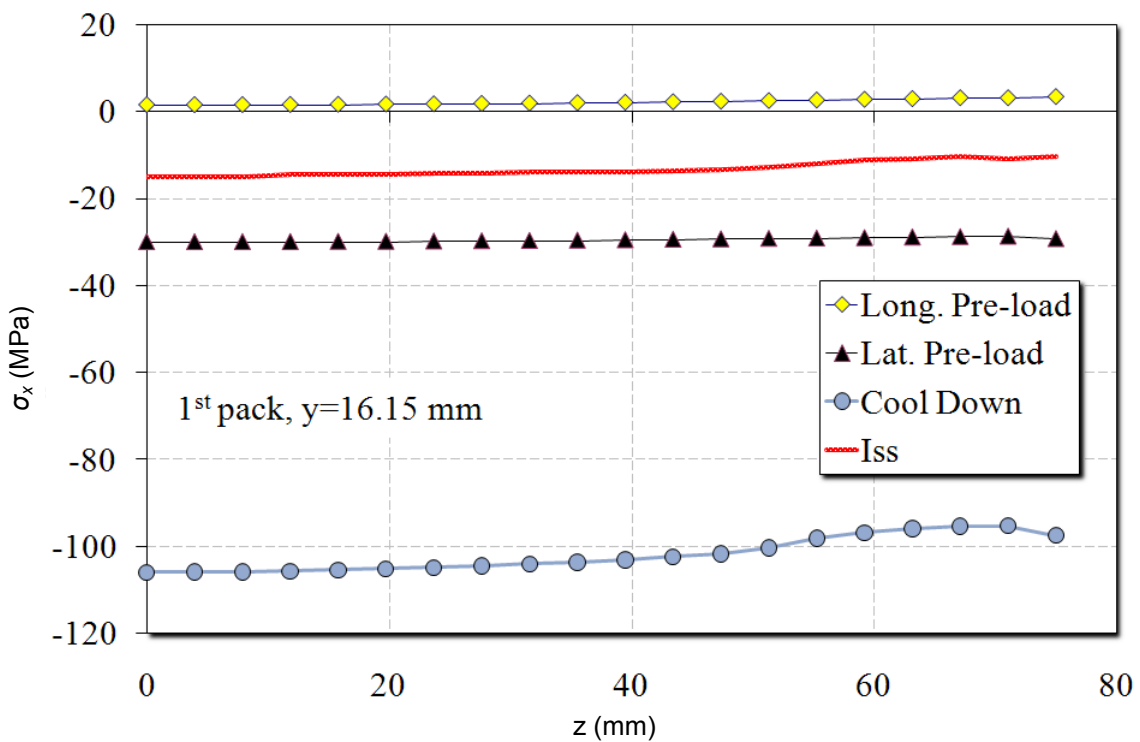
The stress profile along the first cable, where the peak field occurs, is analyzed more in detail in figures 3.7.9 and 3.7.10. Two positions have been taken into account: in the centre of the first cable in the lower and upper layer respectively. The stress component acts transversally to the cable broad face; it is defined as σ_x along the cable straight section, and σ_r along the head. This is related to the coordinate systems used to analyze the stress: global Cartesian for the straight section part, and local cylindrical for the head. As it appears from the plots, the stress distribution is homogeneous in the two layers, the difference being less than some percentages. The longitudinal pre-load affects the stress distribution on the heads only, to a maximum compressive stress of about 50 MPa.

As soon as the lateral pre-load is applied, the difference in stress is smothered over a value of about 40 MPa in compression, all along the contact surface with the main post. The stress level increases at cryogenic temperature to 100 MPa, keeping the same homogeneous distribution as after assembly. The raise in Lorentz forces leads to a decrease in the transverse stress along the pack: a minimum value of 15-20 MPa of uniform compression occurs along the straight section, decreasing to some MPa in correspondence of the magnet symmetry plane.

At end, the full mechanical analysis performed together with CAST3M and ANSYS shows that the SMC structure is safe with the above-mentioned parameters, as well in terms of conductor behaviour than of structural resistance. Before applying our simulation results to the real assembly, a series of validation tests will be performed using specific components. This will help calibrating the strain measurement system and confirming the computational predictions before utilizing them to preload the magnet (see § 4.1.d).

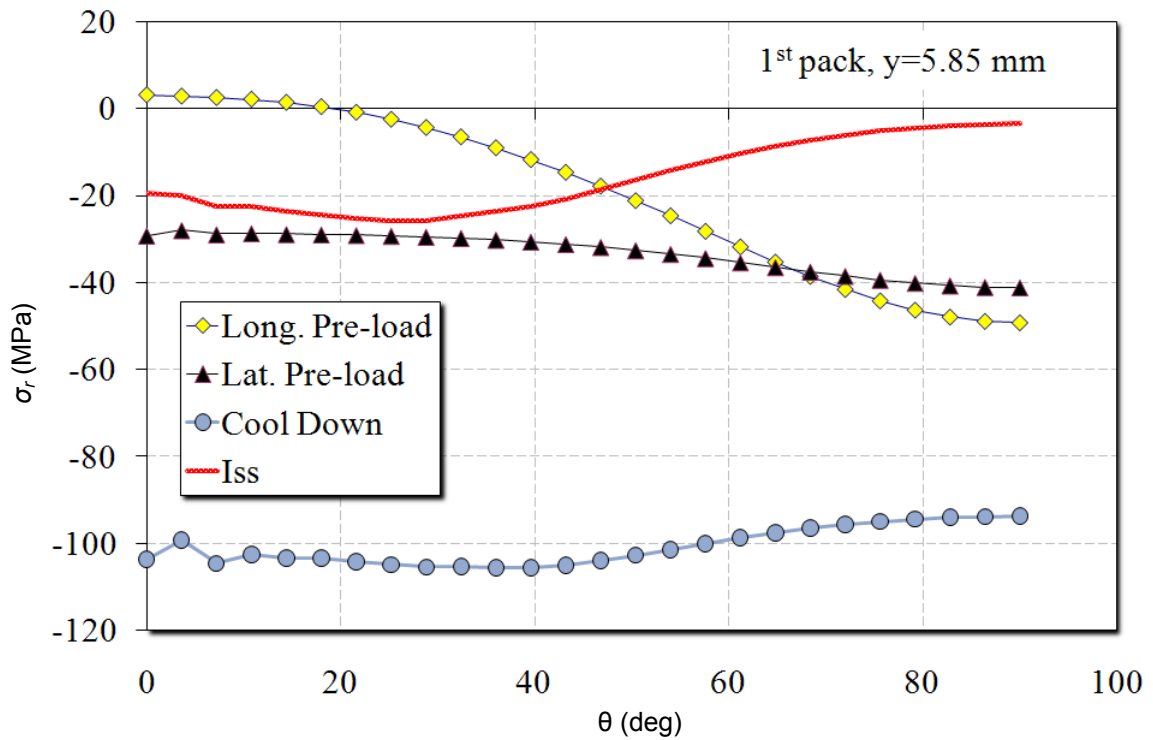


(a)

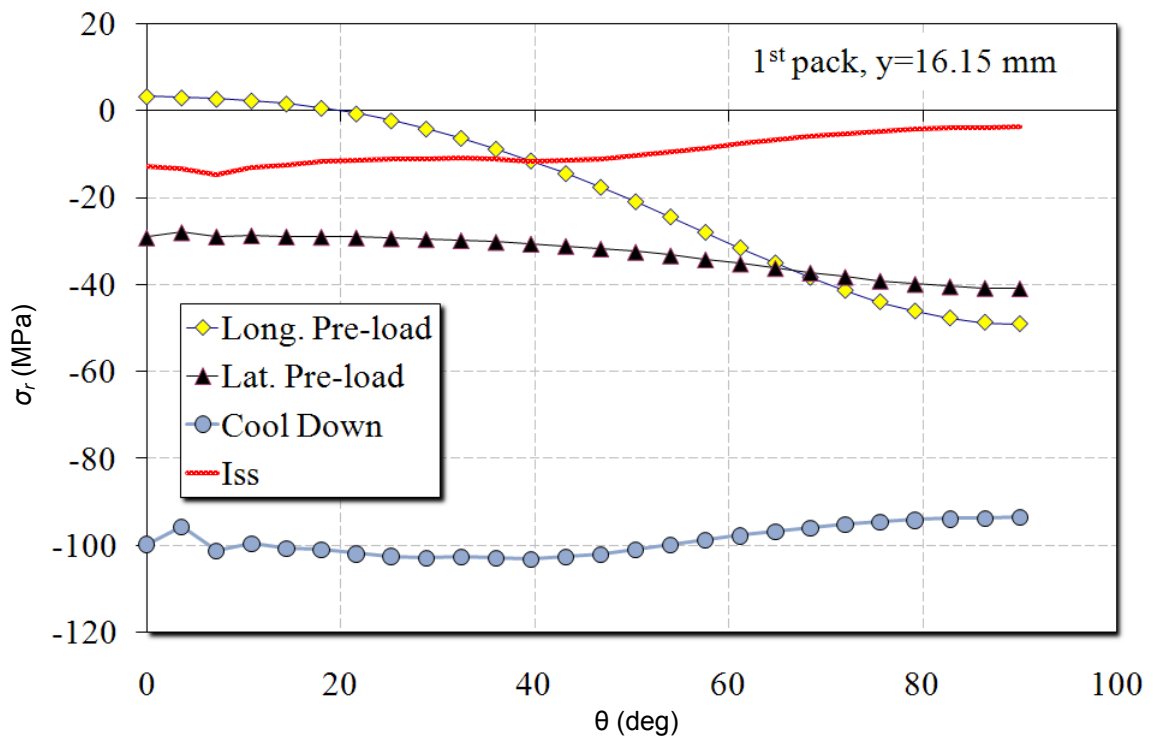


(b)

Fig. 3.7.9: σ_x along the straight section at the coil-pole side: (a) lower layer and (b) upper layer (ANSYS)



(a)



(b)

Fig. 3.7.10: σ_r along the coil head at the coil-pole side: (a) lower layer and (b) upper layer (ANSYS)

4- Detailed Design

4.1- Structure

a. Sub-elements

The SMC structure as described above separates into five packs:

- the outer shell
- the yoke halves (x2)
- the pads (2 X-pads and 2 Y-pads)
- the longitudinal pre-load system
- the bladders (x8)

To be complete, we should add the mechanical tooling (keys, slipshims, dummy coil pack for tests) and the supports (one for room temperature pre-stress and one for the cryostat). This part shows the technical solutions that have been retained to make our optimized mechanical model come true.

b. Parts shape

The **outer shell** is a simple monolithic tube which allows no welding. It has been machined in a full aluminium piece. Let's remind that its outer diameter is 540 mm and its length is 500 mm following the previous optimizations. Two positioning marks have been engraved for gauges sticking.

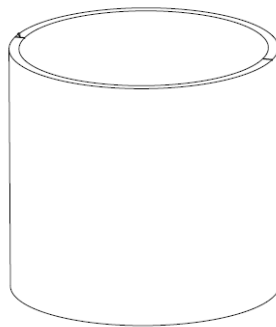


Fig. 4.1.1: outer tube

The **yoke** is composed of two halves. They are made of one central iron part that concentrates the flux, surrounded by two steel parts showing the same profile. It has been proposed to use 5.8 mm-thick LHC iron lamination sheets for the central part, because spare stocks are available at CERN and because their magnetic properties are precisely known. According to our magnetic optimizations [6], 18 layers are necessary. To position and fix them together with the steel parts, a dedicated pin system is proposed. It is represented in green on figure 4.1.2. This system ensures very precise positioning, stack cohesion (with threaded rods) and fluid circulation in case of quenches¹⁰. The yoke halves main surfaces are re-machined after mounting. After this, they are never demounted again. The notch (circled in red) is designed to support the bladders junction bloc (cf. § 4.2).

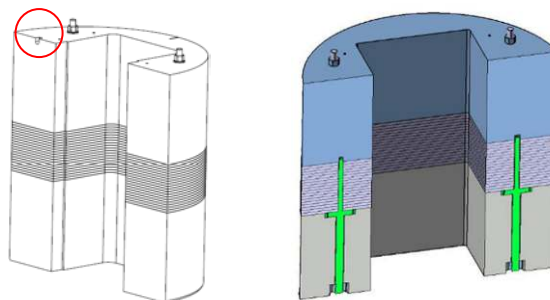


Fig. 4.1.2: half-yoke

¹⁰ Closed cavities must be avoided in superconducting magnet structures because they can become high pressure zones in case of quench. In our configuration, no hole is blind.

The **Y-pads** are also composed of two steel parts around an iron core. They are directly in contact with the coil pack. To increase the geometrical precision of this contact surface, a one-block iron core has been preferred to an iron sheets stack. Positioning and cohesion of the Y-pads are managed by pins and screws as showed in figure 4.1.3. A notch is machined to support the bladders junction block. A $\varnothing 35$ hole is machined for the longitudinal rods.

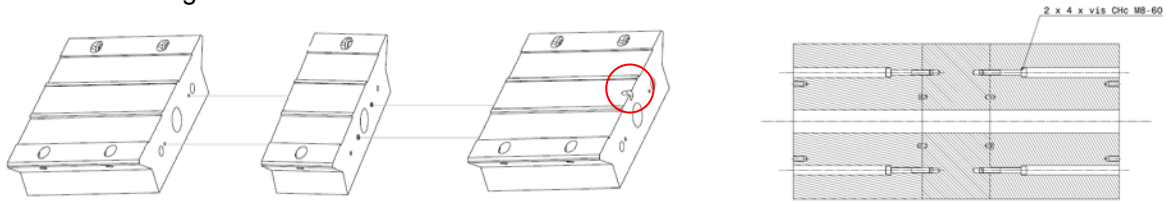


Fig. 4.1.3: Y-pad components

The **X-pads** were initially designed with an iron core too. Nevertheless, this solution is risky because of the first-level role they play during pre-stress: using different materials with different thermal coefficients would lead to a bad pre-stress uniformity. A monolithic part is preferred. Obviously, this supposes to check that the magnetic specifications remain respected. At the same time, it was decided to enlarge the Y-pad to fit with larger coils such as ceramic-insulated one.

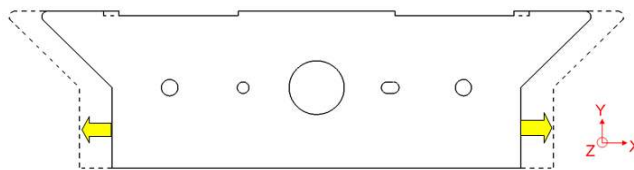


Fig. 4.1.4: Y-pad profile evolution

This modification increases the amount of iron around the coil. We need to show that this effect is sufficient to compensate for an amagnetic X-pad. **The following table shows the main magnetic field features in three cases:**

- CASE 1: 3 piece X-pad (with iron); extended 3 piece Y-pad (with iron): initial solution
- CASE 2: 1 piece X-pad (without iron); extended 3 piece Y-pad (with iron): new solution
- CASE 3: 1 piece X-pad (without iron); 1 piece Y-pad (without iron): witness computation

Parameter	Name	Unit	Specif	values at short sample			Valid
				CASE 1	CASE 2	CASE 3	
Magnetic Field Key Values							
Straight section field	B_{max}	T	≥ 13	12.94	12.91	12.57	OK
				in straight section			
End peak field	B_{end}	T	none	12.27	12.26	12.69	OK
$B_{ss} - B_{end}$	ΔB_{ss}	T	≥ 0.50	0.67	0.64	-0.12	OK CASE 1 / 2
Central field	B_0	T	none	9.91	9.88	8.82	OK
Facilities							
Short sample current	I_{ss}	kA	≤ 20	13.93	14.03	14.82	OK

Tab. 4.1.5: magnetic field with different pad configurations

Also, it is possible to have a monolithic stainless steel X-pad while keeping the magnetic features. Let's remark that every X-pad shows two notches and two grooves to support the bladders.

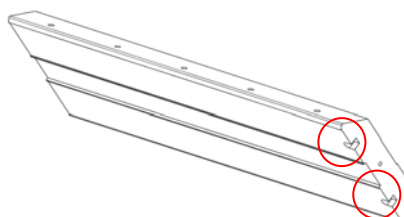


Fig. 4.1.6: X-pad

The four pads can be assembled together around the coil by screws. Those screws are designed not to interfere with the structure behaviour in use. The utile aperture has been set to 50x250 mm, which fixes the insulated horseshoe envelope to **50 x 250 x 500 mm**.

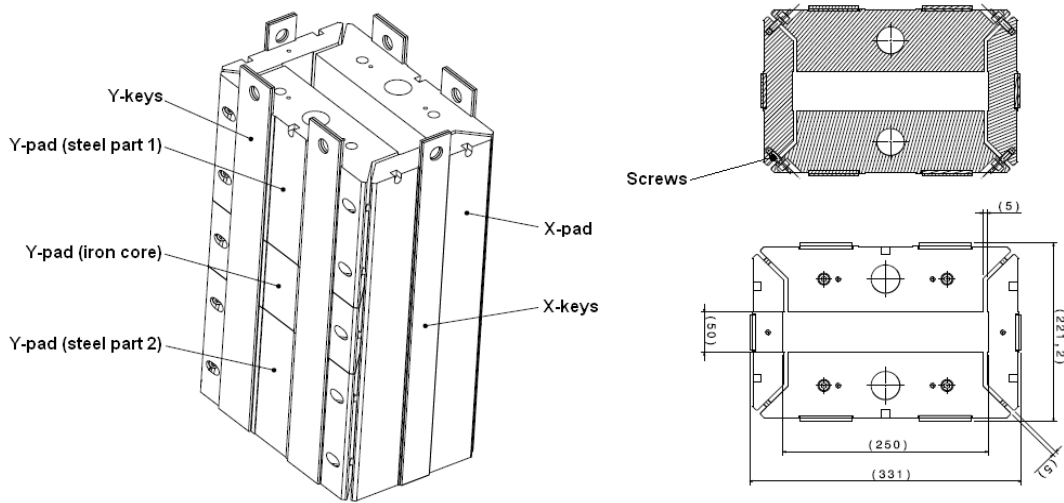


Fig. 4.1.7: pads assembly

The longitudinal rods diameter is 30 mm. They are pre-stressed at room temperature by a hydraulic piston. The nominal pre-stress force corresponds to 50 Tons. Anyway, to remain as flexible as possible, the load system has been designed so that to work also with a 20 Tons piston.

c. Machining tolerances

Target tolerances are very fine on the loading surfaces. According to our models, a dimensional imprecision of 0.1 mm would lead to a difference of ~10 MPa on the coil that we cannot afford. All the composite parts (Y-pads and half-yokes) have been re-machined after assembly.

d. Validation

The structure needs to be instrumented. Indeed, the shell strain is our indicator to control the pre-stress at room temperature and to define the bladders pressure. Before testing the magnets, validation tests will be performed with an instrumented full-block dummy coil pack so that to check the relation between shell strain, coil strain, rods strain and bladders pressure.

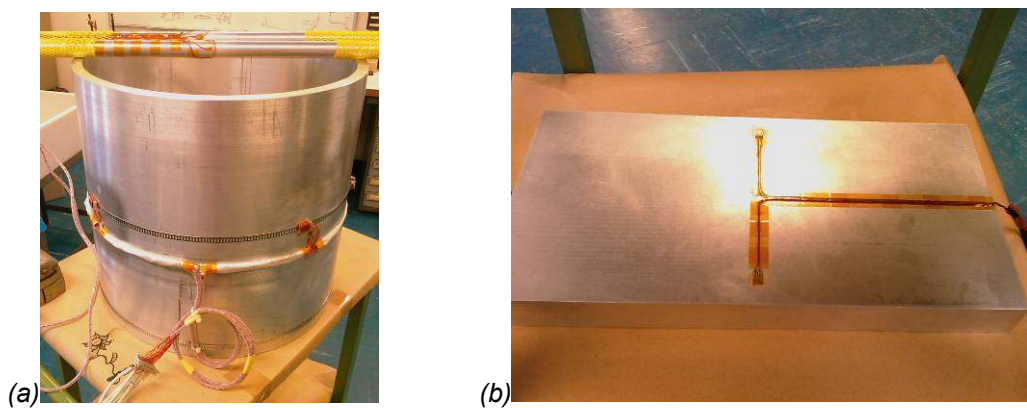


Fig. 4.1.8: structure instrumentation (a) shell (b) dummy aluminium coil pack

This strain gauges instrumentation will consist in:

- on the shell: 4 half-bridges in the longitudinal direction and 4 in the azimuthal direction, with temperature compensation
- on the rods: 1 full-bridge for traction/compression and 1 half-bridge for flexion measurement on each rod
- dummy coil pack: 2 quarter-bridges with compensation gauges in both principal directions

The coil pack instrumentation will be described in another note.

4.2- Bladders

a. Series 1

A first series of bladders (B1, B2 and B3) has been tested in May 2008. They were composed of two 0.25 mm-thick steel sheets plus a steel junction block for water arrival, all sealed by laser welding. The provisory sheets dimensions have been set to 60 x 420 mm. A 5 bars-sealing test has been performed by the supplier without any support causing initial deformations up to 16 mm and weld leakages for B1 and B2.



Fig. 4.2.1: first set of bladders as received from the manufacturer

After press flattening and TIG re-welding, a characterization test has been led, using an appropriate testing device as shown in picture 4.2.4 [14]. It has led to the following conclusions:

Bladder B1 has reached 350 bars for an insertion gap of 2 mm. The leak occurred along the long edge.

Bladder B3 has reached 370 bars for an insertion gap of 2 mm. The leak occurred around the block.

Bladder B2 has leaked at very low pressure around the arrival tube. It has not been considered as meaningful.

Bladder #	5-bars leak test	Initial thickness (max, mm)	Re-weld?	Press (T)	Thickness (max, mm)	Initial gap (mm)	Leak pressure (bars)	Leak type	Aperture (µm)	Final thickness (mm)
B1	NOK	12.4	Yes	200	1.1	2.0	350±20	edge	+400	6.5
B2	NOK	14.4	Yes	200	1.1	2.0	immediate	tube	/	/
B3	OK	16.3	No	200	2.0	2.0	370±20	bloc	+400	5.2

Tab. 4.2.2: bladder test #1 results

Our computations show that the target pressure for SMC nominal use is lower than 200 bars (cf. § 3.4). Thus, those preliminary results were considered as encouraging. Nevertheless, it is obvious that the initial deformation imposed to the bladders must have reduced significantly their performance. It was mandatory to order a second series of bladders without deforming sealing test, and to characterize them again.

b. Series 2

A set of three bladders (called B4, B5, B6) has been ordered by Saclay. Their geometrical specifications are the same than B1, B2 and B3. The 5 bars sealing test has been replaced by a tracer-gas test which is not deforming. It has been successful for the three bladders. The initial thicknesses have been controlled to be in agreement with our specifications: 0.65 ± 0.01 mm in the centre. For every bladder, the characterization process follows two steps: at first a non-destructive test with low initial deformation; then a destructive test with higher deformation.

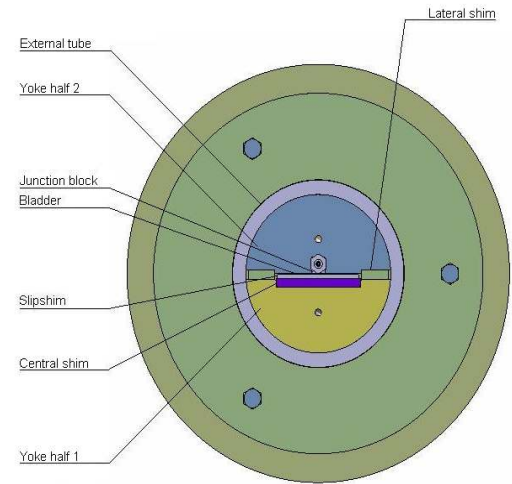


Fig. 4.2.3: bladder test #2 assembly

Fig. 4.2.4: testing device principle

The **non-destructive test** is made with small insertion gaps around the bladders (between 0 and 2 mm) so that their initial deformation remains limited. The goal is to plot the gap aperture as a function of the water pressure. The gap aperture is locked by lateral shims (green in picture 4.2.4) with a resolution of 100 μ m. The test is carried out until the hand pump limit, around 700 bars. The water pressure is gradually increased till the insertion of the successive lateral shims by steps of 100 microns. The insertion pressures given here correspond to the mean values observed for both shims.



Fig. 4.2.5: aperture evolution for B4, B5, B6 plus B1, B3 and theoretical

Bladder #	Tracer-gas leak test	Initial thickness (max, mm)	Initial gap (mm)	Leak pressure (bars)	Leak type	Aperture (μ m)	Final thickness (mm)
B4	OK	0.65	0.0 / 2.0	700 \pm 20	No leak	+600 / NC	2.21 / 3.63
B5	OK	0.65	2.0	700 \pm 20	No leak	+500	NC
B6	OK	0.66	2.0	700 \pm 20	No leak	+500	NC

Tab. 4.2.6: non-destructive bladder test: results summary

First conclusion is that under these conditions **the three bladders have been able to sustain very high pressures, up to 700 bars**. We observe that the shims insertion pressure (full line plots) is not exactly equal to their removal pressure (dotted plots): differences up to 100 bars can be observed, showing the importance of nonlinear effects such as friction and residual deformations. Nevertheless, the slopes remain comparable. The general behaviour of every bladder is similar, with an experimental slope around **0.7 microns/bar**. It is relevant with B1 and B3 results as shown on figure 4.2.5. This shows that the manufacturing process is quite stable. The finite elements theoretical slope, assuming no friction, had been estimated around 1.4 micron/bar (yellow plot). Under pressure, the welds tend to inflate so much that the final bladder thickness is larger than the available gap (*cf.* table 4.2.6, "Final thickness"). This bending effect makes it necessary to use a winch to remove the part, because of friction. **Another option would be to have a vacuum pump available to compress the bladders before removal.**

The **destructive test** aims at pushing every bladder till leakage. It is done without lateral shims. The initial deformation is controlled by the central shim, coloured in violet in picture 4.2.4. Its thickness is progressively decreased, by steps of one millimetre. For each case, the pressure is raised from 1 to 700 bars and then released before increasing the initial gap again. The following table sums up the latest results together with the observations from first series:

Gap	0 mm	2 mm	3 mm	4 mm	Leak type
B1	[not done]	Leak at 350 bars	[broken]	[broken]	edge
B2	[broken]	[broken]	[broken]	[broken]	tube
B3	[not done]	Leak at 370 bars	[broken]	[broken]	bloc
B4	OK till 700 bars	OK till 700 bars	Leak at 110 bars	[broken]	edge
B5	[not done]	OK till 700 bars	Leak at 500 bars	[broken]	edge
B6	[not done]	OK till 700 bars	OK till 700 bars	Leak at 450 bars	edge

Tab. 4.2.7: destructive bladder test: results summary

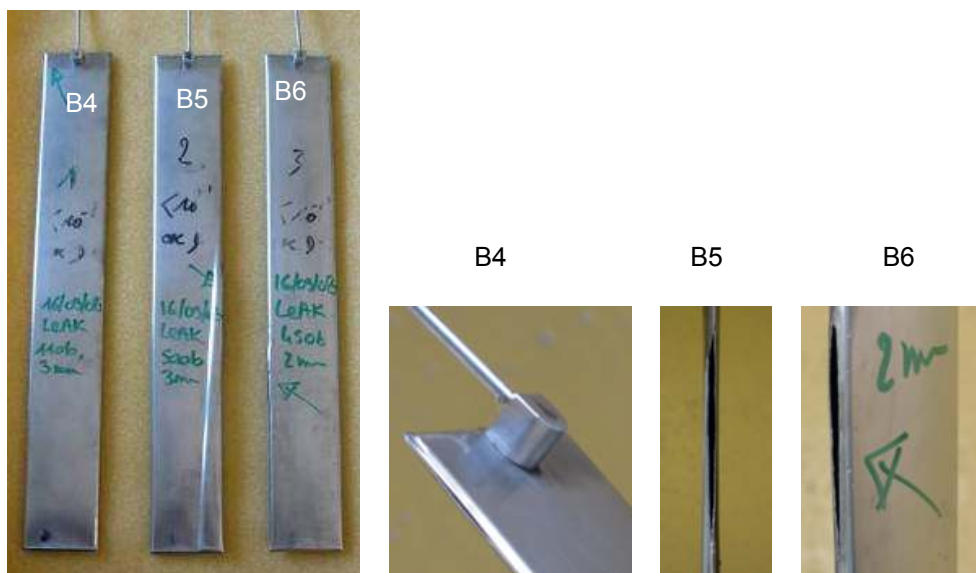


Fig. 4.2.8: bladders from series 2 after leakage (outlook and detail)

The results obtained with B4, B5 and B6 are excellent. The maximum pressures are very large (>700 bars) with gaps under 2 mm. The leaks only appear on edges when high deformations are allowed, larger than 3 mm. Let's remind that target pressure for SMC normal use has been evaluated to 163 bars with a nominal insertion gap of 0.9 mm, corresponding to a final aperture i_x of +300 microns. We can now be sure that this technology gives us a very wide operating margin that will be useful for two reasons:

- we can assume that the bladders will be re-used many times before leakage;
- we will be able to apply easily very high pre-stresses on the short model coils.

4.3- Support and cryostat

To assemble the structure before real tests, a dedicated support has been drawn as shown:

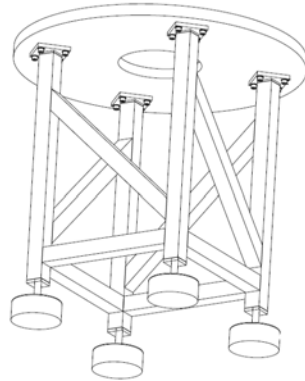


Fig. 4.3.1: support

The cryostat to be used exists at CERN. A rod-supported base plate will be machined to fit in. The structure, held together by friction, will be inserted and tested in vertical position - as on its support.

4.4- Installation procedure

The installation procedure has three phases.

First phase is the **preparation**. It is done on the support at room temperature. The shell is installed first. The yoke halves are assembled in the tube with the yoke bladders (cf. picture 2.1.1) at low pressure (<10 bars). In parallel, the pads assembly can be screwed around the coil pack so that the whole pack is held together by friction. This "pads + coil pack" is inserted in the yoke by sliding along the nominal Y-keys on one side. The nominal keys correspond to the best guess of what you expect in terms of final key size (key + shims). Then the bladders are inserted and the missing nominal keys are put around the coil pack with or without the help of the bladders. The shimming is increased using the X and Y-bladders until the coil pack is tight in the yoke cavity.

Next phase is the **pre-stress at room temperature**, performed on the same support. It consists first in preloading longitudinally the magnet by pre-tensioning the rods. This is done with a commercial hydraulic piston¹¹. Finally, the remainder of the axial pre-stress is applied with the help of the X-bladders by shimming the loading keys in accordance with the target shell strain at room temperature (monitored with strain gages). The target strain level is locked by the appropriate shim before deflating and removing the bladders. A practical 50 µm-clearance is necessary for shim insertion. Several bladders can be pressurized at the same time.

The magnet assembly should at this stage behave as a one part. It can be transported from the support table to the cryostat so that the electrical connections are set up for the tests.

¹¹ The support is designed for ENERPAC® RSM-200 (20 Tons) or RSM-500 (45 Tons)

5- Conclusions and next steps

This second step of NED SMC project has led to design the mechanical test bed for our Nb₃Sn subscale coil. It makes it possible to pre-stress appropriately the coil so that to keep its inner stresses below 150 MPa after magnetization. At every step of the magnet lifecycle, the stresses remain controlled in every part of the assembly, and particularly on the conductor. At the same time, the pre-load can be offset finely, allowing us to study the mechanical stress dependence of the superconducting cable performances.

Using SD01 as a starting point, SMC study has shown:

- increasing the structure dimensions and limits
- refining the iron inserts location
- optimizing the bladders features to reach higher pressures and higher gaps
- reinforcing the longitudinal support
- allowing different coil shapes for future tests

This mechanical study has been a new occasion to cross-check CAST3M and ANSYS formulations in many cases, improving our know-how in the field of 3D nonlinear magneto-mechanical modelling.

The structural parts, as described in this note, have been machined under control of CEA and delivered to CERN in November 2008. They have been instrumented with strain gauges by CERN. In parallel, RAL has worked on the coil winding process. The coil pack instrumentation, including strain gauges, hall probes and voltage taps, has been looked at by CERN and will be described in another note. The magnet is small enough not to need quench heaters for protection.

The SMC structure is now ready for the cryogenic tests:

- validation tests with the dummy coil pack to check the gauges at room and cryogenic temperature
- Nb₃Sn SMC dipole tests with conventional insulation
- Nb₃Sn HFM dipole tests with ceramic insulation



Fig. 5.1: SMC structure on its support, with dummy coil pack inside

Acknowledgements

The SMC working group would like to thank everyone involved in the mechanical optimization described in this paper, especially Noël Dalexandro at CERN for his support with coils winding, Michel Guinchard for the structure instrumentation and the related pictures, Françoise Rondeaux, Thomas Dalla-Foglia and Aubrey Poulizac at Saclay for the bladders tests, and Philippe Daniel-Thomas and Thierry Lerch (also at Saclay) for the structural parts drawing and drafting. Thank you very much to François Nunio (CEA/IRFU/SIS) for his support in CAST3M modelling. We would like to acknowledge again every people involved in the previous magnetic optimization phase: James Rochford, Arnaud Devred, François-Paul Juster, François Nunio and Pierre Védrine.

Tables and figures

Type	#	Name	Courtesy
Fig.	1.2.1	SMC magnet optimized geometry	P. Manil
Tab.	1.2.2	SMC magnetic optimization results	SMC working group
Fig.	1.2.3	SMC expected magnetic field at short sample	P. Manil
Tab.	1.2.4	magnetic forces and energy at short sample	SMC working group
Fig.	2.1.1	SMC mechanical baseline structure (2D cut)	F. Nunio, P. Manil
Tab.	3.1.1	SMC material properties	SMC working group
Fig.	3.2.1	SMC main parameters in 2D	P. Manil
Fig.	3.3.1	CAST3M mechanical mesh	P. Manil
Fig.	3.3.2	boundary conditions and contacts in CAST3M	P. Manil
Fig.	3.3.3	mechanical computation diagram in CAST3M	P. Manil
Fig.	3.3.4	ANSYS 2D mechanical mesh	F. Regis
Fig.	3.4.1	i_x and t_{shell} influence on coil lateral pressure before magnetization	P. Manil
Fig.	3.4.2	Lorentz 2D nodal forces and resulting axial stresses map allure	P. Manil
Fig.	3.4.3	visualisation of the coil/pole/spacers separations in a particular case	P. Manil
Fig.	3.4.4	SMC lifecycle after 2D optimization in CAST3M	P. Manil
Fig.	3.4.5	$\sigma_{VM,max}$ as a function of i_x in ANSYS	F. Regis
Fig.	3.4.6	t_{shell} as a function of w_{yoke} in ANSYS with the above-mentioned criteria	F. Regis
Fig.	3.5.1	coil pack 3D modelling	P. Manil
Fig.	3.5.2	coil pack behaviour at 14 kA without longitudinal support	P. Manil
Tab.	3.5.3	radial stresses on coil edges in 2D and in simplified 3D for different i_z	P. Manil
Tab.	3.6.1	structure deformation and Von Mises coil stresses for different i_z	P. Manil
Tab.	3.6.2	optimized structure lifecycle (CAST3M)	P. Manil
Fig.	3.7.1	ANSYS 3D mechanical model	F. Regis
Fig.	3.7.2	conductor meshes in ANSYS for the magnetic/mechanical models	F. Regis
Fig.	3.7.3	$\sigma_{r,max}$ on the inner coil head as a function of the d_z (ANSYS)	F. Regis
Tab.	3.7.4	3D assembly and pre-load parameters	SMC working group
Fig.	3.7.5	σ_{VM} in the longitudinal rods after assembly and powering (ANSYS)	F. Regis
Fig.	3.7.6	σ_r evolution in the inner coil head at each step (ANSYS)	F. Regis
Fig.	3.7.7	σ_{VM} in the coil pack after cool-down and powering (ANSYS)	F. Regis
Tab.	3.7.8	SMC 3D model results in ANSYS	F. Regis
Fig.	3.7.9	σ_x along the straight section at the coil-pole side (ANSYS)	F. Regis
Fig.	3.7.10	σ_r along the coil head at the coil-pole side (ANSYS)	F. Regis
Fig.	4.1.1	outer tube	Th. Lerch
Fig.	4.1.2	half-yoke	Ph. Daniel-Thomas
Fig.	4.1.3	Y-pad components	P. Manil
Fig.	4.1.4	Y-pad profile evolution	P. Manil
Tab.	4.1.5	magnetic field with different pad configurations	P. Manil
Fig.	4.1.6	X-pad	Th. Lerch
Fig.	4.1.7	pads assembly	Th. Lerch
Fig.	4.1.8	structure instrumentation: shell - dummy aluminium coil pack	M. Guinchard
Fig.	4.2.1	first set of bladders as received from the manufacturer	P. Manil
Tab.	4.2.2	bladder test #1 results	P. Manil
Fig.	4.2.3	bladder test #2 assembly	P. Manil
Fig.	4.2.4	testing device principle	P. Manil
Fig.	4.2.5	aperture evolution for B4, B5, B6 plus B1, B3 and theoretical	P. Manil
Tab.	4.2.6	non-destructive bladder test: results summary	P. Manil
Tab.	4.2.7	destructive bladder test: results summary	P. Manil
Fig.	4.2.8	bladders from series 2 after leakage (outlook and detail)	P. Manil
Fig.	4.3.1	support	Th. Lerch
Tab.	5.1	SMC Structure on its support, with dummy coil pack inside	P. Manil

Acronyms and symbols

Symbol	Meaning
AT	Accelerator Technologies
CARE	Coordinated Accelerator Research in Europe
CEA	Commissariat à l'Énergie Atomique
CERN	European Organization for Nuclear Research
<i>d.o.f.</i>	Degree Of Freedom
FE	Finite Elements
IRFU	Institut de Recherche sur les lois Fondamentales de l'Univers
JRA	Joint Research Activity
LARP	LHC Accelerator Research Program
LBNL	Lawrence Berkeley National Laboratory
LHC	Large Hadron Collider
NED	Next European Dipole
RAL	Rutherford Appleton Laboratory
ROXIE	Routine for the Optimization of magnet X-sections, Inverse field computation and coil End design
RT	Room Temperature
SACM	Service des Accélérateurs et du Cryo-Magnétisme
SD01	Subscale Dipole #1
SIS	Service d'Ingénierie des Systèmes
SMC	Short Model Coils
TE	Technology department
UTS	Ultimate Tensile Stress
ΔB_{ss}	Difference between straight section and end peak fields at short sample current
ΔT	Difference between room and cryogenic temperatures (typically 289 K)
σ_x, σ_r	Principal stress in the X/radial-direction
σ_{VM}	Equivalent Von Mises stress
σ_{lim}	Limit admissible stress
\varnothing_{rod}	Rod diameter
B_0	Central magnetic field
B#	Bladder name
B_{max}	Peak magnetic field
B_{end}	End peak magnetic field
d_z	Longitudinal pre-load displacement
h_{coil}	Coil pack thickness
E_{mag}	Total stored magnetic energy (on full magnet)
e_{tot}	Overall thickness
e_{tube}	<i>see t_{shell}</i>
F_x, F_y, F_z	Force component on 1/8 th coil
F_x^{2D}, F_y^{2D}	Force component on straight section
I_{ss}	Short sample current
i_x, i_y	Bladder interferences
i_z	Longitudinal pre-load interference
L	Straight section length (on inner pack)
\mathcal{L}	Magnet inductance
L_{blad}	Bladder length
L_{int}	Outer spacer axial length
L_s	Inner spacer axial length
L_{tot}	Overall length
N_{int}	Inner turns number
N_{mid}	Mid-pack turns number
N_{out}	Outer turns number
N_{tot}	Total turns number
O_x, O_y, O_z	Axes
P_{blad}	Water pressure in the bladders
r_{int}	Island half-width
r_{out}	Outer radius
r_{yoke}	Yoke radius
t_{shell}	Shell thickness
W_{hs}	Horseshoe lateral width
W_{tot}	Overall width
W_{yoke}	Yoke thickness ($W_{yoke} = r_{yoke} - 140$ mm)
Z_{x-pad}	X-pad iron longitudinal extension
Z_{y-pad}	Y-pad iron longitudinal extension
Z_{yoke}	Yoke iron longitudinal extension

References

[1] **A. DEVRED *et al.***

Overview and status of the Next European Dipole Joint Research Activity
Supercondu. Sci. Technol. 19 (2006) S67-S83

[2] **S. CASPI, S. GOURLAY, R. HAFALIA, A. LIETZKE, J. ONEILL, C. TAYLOR, A. JACKSON**

The use of pressurized bladders for stress control of superconducting magnets
IEEE Transactions on Applied Superconductivity, Vol. 11, No. 1, March 2001

[3] **R.R. HAFALIA, S. CASPI, L. CHIESA, M. COCCOLI, D.R. DIETDERICH, S. A. GOURLAY, A.F. LIETZKE, J.W. O'NEILL, G. SABBI, AND R.M. SCANLAN**

A new support structure for high field magnet
IEEE Transactions on Applied Superconductivity, Vol. 12, No. 1, March 2002, pp. 47-50

[4] **R.R. HAFALIA, P.A. BISH, S. CASPI, D.R. DIETDERICH, S.A. GOURLAY, R. HANNAFORD, A.F. LIETZKE, N. LIGGINS, A.D. MCINTURFF, G.L. SABBI, R.M. SCANLAN, J.W. O'NEILL, J.H. SWANSON**

An approach for faster high field magnet technology development
IEEE Transactions on Applied Superconductivity, Vol. 13, No. 2, June 2003, pp. 1258-1261.

[5] **F. RONDEAUX**

Insulation development: final report on innovative insulation
CARE-Report-2007-037-NED, Dec. 2007, CEA Saclay, France

[6] **P. MANIL, F. REGIS, J. ROCHFORD *et al.***

NED Short Model Coils project: Technical note on magnetic design
CEA/CERN Internal report, EDMS id.: 926137, June 2008

[7] **H. FÉLICE**

Contribution à la conception des bobinages supraconducteurs de type dipolaire en Nb₃Sn pour les accélérateurs de particules
Rapport de thèse CEA DAPNIA-06-09-T; thèse soutenue le 12/10/2006

[8] **H. FÉLICE *et al.***

Design and test of a Nb₃Sn subscale dipole magnet for training studies
IEEE Transactions on Applied Superconductivity, Vol. 17, Issue2, Part 2, June 2007

[9] **P. LOVERIDGE *et al.***

Mechanical properties for NED SMC computations
CERN Internal report, EDMS id.:683000

[10] **P. VERPEAUX, T. CHARRAS, A. MILLARD**

Castem2000: une approche moderne du calcul des structures
in Calcul des Structures et Intelligence Artificielle, p. 261. Pluralis, 1988

[11] **ANSYS USER GUIDE**

[12] **F. REGIS**

Design of Nb₃Sn devices to study the superconductor degradation under variable mechanical load
PhD thesis, to be defended in June 2009

[13] **P. MANIL**

Short Model Coils meeting #16
CEA presentation, internal document, EDMS id.: 882446, November 2007

[14] **P. MANIL**

NED Short Model Coils project: Technical description of the Bladder Testing Device
CEA Internal report, SMC-TD-01, March 2008

Internet references:

[i.1] <http://lt.tnw.utwente.nl/research/HCS/Projects/CARE-NED/>

Official CARE-NED project homepage

[i.2] <https://edms.cern.ch/>

NED SMC Project database; note, presentations and Minutes available [restricted access]